AGU PUBLICATIONS

Geochemistry, Geophysics, Geosystems

RESEARCH ARTICLE
10.1002/2014GC005483

Companion to *Tesauro et al.* [2014], doi:10.1002/2014GC005484.

- Gravity and seismic tomography data are jointly inverted using a new technique
- A 3-D density model of the North American upper mantle is obtained
- The results constrain the origin of the upper mantle heterogeneity

Correspondence to:
M. K. Kaban,
kaban@gfz-potsdam.de

Citation:
Kaban, M. K., M. Tesauro, W. D. Mooney, and S. A. P. L. Cloetingh (2014), Density, temperature, and composition of the North American lithosphere—New insights from a joint analysis of seismic, gravity, and mineral physics data: 1. Density structure of the crust and upper mantle, *Geochem. Geophys. Geosyst.*, *15*, 4781–4807, doi:10.1002/2014GC005483.

Received 16 JUL 2014
Accepted 16 NOV 2014
Accepted article online 20 NOV 2014
Published online 10 DEC 2014

Density, temperature, and composition of the North American lithosphere—New insights from a joint analysis of seismic, gravity, and mineral physics data: 1. Density structure of the crust and upper mantle

Mikhail K. Kaban[1,5], Magdala Tesauro[1,2], Walter D. Mooney[3], and Sierd A. P. L. Cloetingh[2,4]

[1]GeoForschungsZentrum Potsdam, Potsdam, Germany, [2]Department of Earth Sciences, Utrecht University, Utrecht, Netherlands, [3]USGS, Menlo Park, California, USA, [4]Ludwig-Maximilians University of Munich, Munich, Germany, [5]Geophysical Center, IPE, RAS, Moscow, Russia

Abstract We introduce a new method to construct integrated 3-D models of density, temperature, and compositional variations of the crust and upper mantle based on a combined analysis of gravity, seismic, and tomography data with mineral physics constraints. The new technique is applied to North America. In the first stage, we remove the effect of the crust from the observed gravity field and topography, using a new crustal model (NACr2014). In the second step, the residual mantle gravity field and residual topography are inverted to obtain a 3-D density model of the upper mantle. The inversion technique accounts for the notion that these fields are controlled by the same factors but in a different way, e.g., depending on depth and horizontal dimension. This enables us to locate the position of principal density anomalies in the upper mantle. Afterward, we estimate the thermal contribution to the density structure by inverting two tomography models for temperature (NA07 and SL2013sv), assuming a laterally and vertically uniform "fertile" mantle composition. Both models show the cold internal part and the hot western margin of the continent, while in some Proterozoic regions (e.g., Grenville province) NA07 at a depth of 100 km is $>200^{\circ}$C colder than SL2013sv. After removing this effect from the total mantle anomalies, the residual "compositional" fields are obtained. Some features of the composition density distribution, which are invisible in the seismic tomography data, are detected for the first time in the upper mantle. These results serve as a basis for the second part of the study, in which we improve the thermal and compositional models by applying an iterative approach to account for the effect of composition on the thermal model.

1. Introduction

The North American (NA) continent is composed of several tectonic provinces, each with a different age and geologic evolution. Most of the central and eastern part of the continent has been relatively stable since the mid-Proterozoic [e.g., *Hoffman*, 1997], while the western part is a broad, actively deforming region extending from Mexico to Alaska [e.g., *Dickinson*, 2004]. Density heterogeneity of the upper mantle largely controls tectonic processes in the overlying crust. At the same time, all density perturbations occurring in the lithosphere are the result of geodynamic processes, such as mountain building and plume upwelling. Therefore, knowledge of density variations in the uppermost mantle is essential for understanding the evolution of the NA continent. In particular, it is important to assess the two main physical parameters that are mainly responsible for the density changes: temperature and composition. In turn, their knowledge offers the opportunity to estimate other physical properties (e.g., rheology) of the lithosphere.

Despite a large number of studies on the structure of the crust and uppermost mantle of North America [e.g., *Grand*, 1994; *Godey et al*., 2003; *Nettles and Dziewonski*, 2008; *Bedle and van der Lee*, 2009; *Yuan et al.*, 2011], several key issues are still open. One important problem is the separation of the effects of thermal and compositional anomalies in various geophysical fields (primarily in gravity and seismic tomography). Previous studies [e.g., *Deschamps et al*., 2002] linked seismic velocity to density perturbations in the upper mantle through relative scaling of the conversion factor ($R\rho/s = dln\rho/dlnV_s$). Using this approach, *Godey et al*. [2004] tried to estimate both temperature and compositional variations in the upper mantle of NA. They expressed mineralogical variations in the mantle in terms of the volumetric fraction of iron, the

parameter which has the strongest correlation of the major elements with density and velocity [e.g., *Jordan*, 1979]. The authors reached the conclusion that the upper mantle of the cratons at a depth of 100 km is cooler by ~440 K and depleted in *Fe* by ~4% relative to the average temperature of 1100 K and an iron fraction of 11%. In subsequent studies, this method has been further developed by applying a probabilistic approach aiming to invert seismological data directly into thermo-chemical structure [e.g., *Khan et al*., 2011]. More specifically, the authors use a Markov Chain Monte Carlo method to estimate the thermo-chemical, physical, and anisotropic structure beneath the NA continent using the global surface wave phase-velocity maps of *Visser et al*. [2008]. They obtained a range of tomographic, thermal, and compositional models of the NA mantle, the latter in terms of Mg# ($100 \times Mg/(Mg + Fe)$). Their results confirmed that the cratonic mantle is characterized by depletion in *Fe* and lower temperatures relative to the active younger regions in the western part of NA. The main drawback of this approach is that several parameters are estimated based on variations of only one physical parameter (seismic velocity or phase-velocity maps). Therefore, the solution that is obtained always represents just one of an infinite number of possible solutions. Other fields (e.g., gravity or geoid) are used only for comparison with the preferred results [e.g., *Khan et al*., 2011].

We employ a joint interpretation of seismic, gravity, and other available data (e.g., topography), in order to overcome the problem of nonuniqueness in geophysical inversions. *Mooney and Kaban* [2010] applied a subsequent back stripping of the observed gravity field aiming to identify the component of the gravity field that reflects density variations in the upper mantle, and to determine the role of the different factors (thermal versus composition) controlling lateral density variations. In the initial step, they constructed a density model of the crust. Available seismic data have been used to estimate the Moho depth and variations of *P* wave average velocities in the crystalline crust. These crustal velocities were converted to densities using experimentally determined relationships [*Christensen and Mooney*, 1995]. The thickness and density of the sedimentary basins have been determined from published maps and summaries of borehole measurements. These crustal data have been used to estimate the gravity effect of the crust and to remove it from the observed gravity field. The residual mantle gravity anomalies obtained in this way reflect the density structure of the mantle. A comparison of the mantle anomaly map with the topographic map indicates that a significant amount of the topographic uplift in western NA is due to buoyancy in the hot upper mantle. The analysis of the gravity and topographic data, as described above, indicates that the buoyancy contribution of the upper mantle is very significant and different from that predicted from seismic tomography images. In order to separate the contributions of temperature anomalies from mantle composition, an additional correction for the thermal structure of the uppermost mantle has been applied. The thermal model used to estimate the thermal component of the mantle gravity anomalies was obtained from *Goes and van der Lee* [2002] from the inversion of the tomography model NA00 [*van der Lee and Nolet*, 1997] in temperature through a mineral physics approach. The thermally corrected residual map reveals mantle density anomalies that should be due to compositional variations if all the applied corrections are accurate. A preliminary analysis confirms that some of the prominent features are consistent with our knowledge about properties of the upper mantle, such as the low densities related to *Fe* depletion, that characterize the cratonic regions.

Despite these encouraging results, several important issues remain open. The principal question is: how reliable is the estimated upper mantle thermal structure obtained using seismic tomography? Up to now, it was difficult to assess uncertainties of the conversion from seismic velocities to temperature [e.g., *Tesauro et al*., 2012a]. Indeed, seismic velocities mainly depend on temperatures, but other effects, such as compositional variations also play an important role [e.g., *Goes et al*., 2000]. The thermal model of *Goes and van der Lee* [2002] was estimated using a uniform composition. However, the ability to fit the seismic velocities purely in terms of thermal variations does not exclude the presence of compositional variations. Neglecting these variations might lead to significant errors in the estimations of temperature [e.g., *Afonso et al*., 2010; *Hieronymous and Goes*, 2010]. In addition, different tomography models often give substantially different velocity variations, depending on the data and assumption used in the seismic inversion [e.g., *Bedle and van der Lee*, 2009]. In particular, the reference velocity models used in the tomography inversion are often different [e.g., *Cammarano et al*., 2011]. For instance, the tomography models that use PREM [*Dziewonski and Anderson*, 1981] as a reference model (e.g., S40RTS of *Ritsema et al*. [2011]) display strong velocity changes at a depth of 220 km. Such a discontinuity does not exist globally and is not

required beneath continental regions, as many other models demonstrate [e.g., *Deuss*, 2009]. The artificial effect of this 220 km discontinuity might propagate in the temperatures estimates obtained from inversion of seismic velocities. Therefore, the lateral velocity variations provided by seismic tomography may be more reliable than their absolute values, which are required for temperature estimations, particularly on account of the nonlinearity in the relation between velocity and temperature introduced by anelasticity [*Goes et al*., 2000].

It should be also noted that the NA mantle density model of *Mooney and Kaban* [2010] does not provide a density-depth distribution. In fact, the compositional density variations refer to a homogeneous 100 km thick layer. In addition, the model of the crystalline crust used in that study provides only averaged values of velocities and densities. It is likely these assumptions do not lead to significant errors in the mantle gravity anomalies, but the influence of these assumptions should be evaluated, as we have done here.

In the present study, we aim to create a density model of the NA crust and upper mantle that is based on newly improved interpretation methods and initial data sets. The integrated 3-D model of the NA lithosphere and upper mantle will yield density variations associated with temperature and compositional anomalies which are estimated through an iterative inversion. We also analyze potential errors of the model related to both uncertainties of the initial data and of the method used. The main advances compared to previous studies are the following:

1. A new improved model of the crust (NACr2014) [*Tesauro et al*., 2014a] is used to estimate the crustal contribution to the observed gravity field. In comparison with the previous model [*Mooney and Kaban*, 2010], NACr14 provides three layers of the crystalline crust, each with velocity and density variations specified.
2. We use a newly developed inversion technique that uses residual gravity anomalies and residual topography to construct a 3-D density model of the upper mantle.
3. Two recent seismic tomography models [*Bedle and van der Lee*, 2009; *Schaeffer and Lebedev*, 2013] are inverted for mantle temperature to quantify the effect of their differences on the estimated thermochemical structure of the upper mantle.
4. Temperature and compositional anomalies in the upper mantle are determined simultaneously in an iterative approach.

In this first contribution, we present the general concept and discuss the initial density and temperature models of the upper mantle. In the second contribution [*Tesauro et al*., 2014b, this volume], we analyze thermal and compositional models of the upper mantle obtained with the iterative inversion.

2. Study Area

The study area is delimited by the coordinates 10°N by 85°N and 170°W by 50°W and includes most of the NA continent (Figure 1), which is composed of Archean and Proterozoic cratonic blocks, flanked by Phanerozoic Orogenic belts. In the central and eastern part of the NA continent, there are several Archean cratons, such as the Slave, Churchill, Superior, and Wyoming cratons, composing the large Laurentia block [e.g., *Bleeker*, 2003]. These Archean cratons have been assembled during the Proterozoic Eon (from 1.8 to 0.8 Ga) by the accretion of additional terrains to the southern and western edges of Laurentia during the creation and dispersal of the supercontinent Rodinia [e.g., *Karlstrom and Humphreys*, 1998]. Phanerozoic tectonic processes, such as the accretion of the Appalachian Mountains on the east coast during the Paleozoic and formation in the Mesozoic/Cenozoic of the western Cordillera, which extends from Mexico to Alaska, completed the formation of the continent. According to its geology, tectonics, and structure, the NA continent is roughly divided along the Rocky Mountain Front into the stable eastern and tectonically active western parts. The latter is characterized by high surface heat flow [*Blackwell and Richards*, 2004], generally thin (25–35 km) crust [e.g., *Mooney and Kaban*, 2010] low crustal *Pn* and *Sn* velocities [e.g., *Nolet et al*., 1998; *Tesauro et al*., 2014a] and a low resistivity [e.g., *Rippe et al*., 2013]. All these properties indicate a warm, hydrated uppermost mantle that has been responsible for the high elevations of western North America [e.g., *Mooney and Kaban*, 2010]. In contrast, the eastern part of the continent is characterized by low relief, low surface heat flow [*Blackwell and Richards*, 2004], thicker (35–50 km) crust, and high crustal and shallow mantle velocities [*Tesauro et al*., 2014a; *Bedle and van der Lee*, 2009].

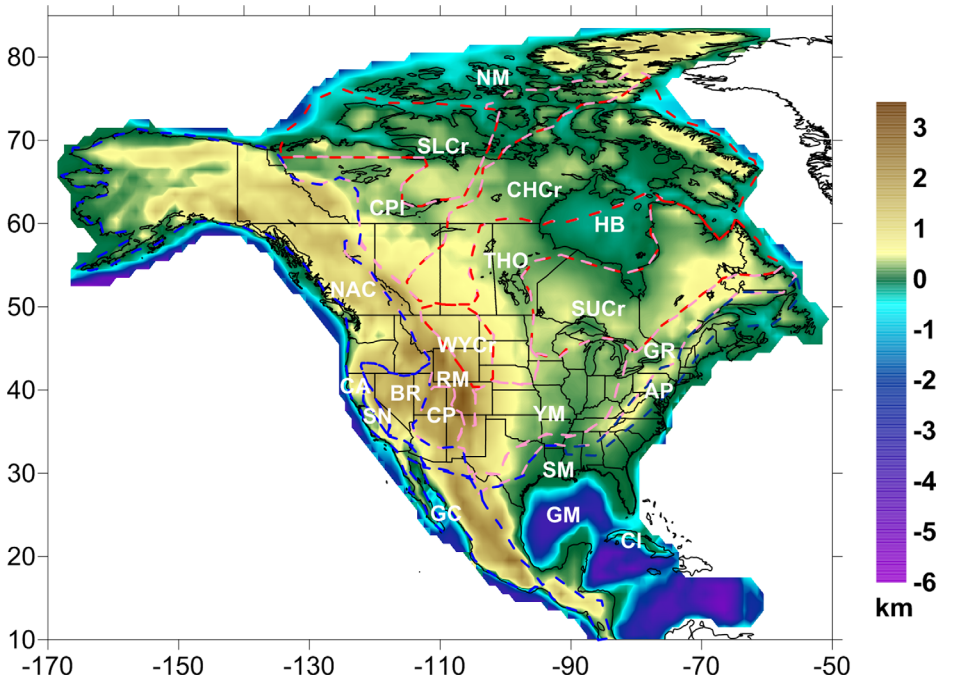

Figure 1. Topographic map of North America (km), taken from ETOPO2 [*NOAA*, 2010]. Red, pink, and blue dashed contours show the boundaries between the Archean, Proterozoic and Phanerozoic tectonic provinces, delineated taking into account the crustal age, the geographical extension of the key tectonic elements and the physiographical boundaries [modified after *Tesauro et al*., 2014a]. White labels stand as follows: **AP**, Appalachians; **BR**, Basin and Range; **CA**, Cascade; **CHCr**, Churchill craton; **CI**, Cuba Island; **CP**, Colorado Plateau; **CPl**, Canadian Platform; **GC**, Gulf of California; **GM**, Gulf of Mexico; **GR**, Grenville; **HB**, Hudson Basin; **NAC**, North American Cordillera; **NM**, North Margin; **RM**, Rocky Mountains; **SLCr**, Slave craton; **SM**, South Margin; **SN**, Sierra Nevada; **SUCr**, Superior craton; **THO**, Trans-Hudson Orogen; **WYCr**, Wyoming Craton; **YM**, Yavapai-Mazatzal province.

3. Modeling Concept

This study employs the following principal modeling steps, which are shown in the diagram (Figure 2):

1. Computation of the crustal gravity effect and its removal from the observed gravity field. Estimation of the residual topography using these results.
2. Joint inversion of the residual gravity and residual topography to produce a 3-D density model of the upper mantle.
3. Initial conversion of seismic velocities in the upper mantle to temperature. At this stage, a uniform composition of the upper mantle is assumed.
4. Computation of the gravity effect induced by temperature variations and its removal from the total mantle gravity anomalies. Application of the same procedure to the residual topography. Joint inversion of these fields and construction of a preliminary density model that identifies compositional variations in the upper mantle.
5. Evaluation of compositional changes using the density model obtained in step 4. Repetition of the steps 3 and 4, but taking into account the compositional changes obtained in the previous step. The iterative loop runs until convergence is reached.

In the next section, we describe the methods used for the gravity modeling.

3.1. Computation of the Crustal Gravity Effect and Residual Topography

The gravity effect of the crust is estimated relative to a laterally homogeneous (1-D) reference density model consisting of several standard layers. The crustal correction is equivalent to replacing of the laterally varying crust with the homogeneous reference crustal model [e.g., *Mooney and Kaban*, 2010]. Thus, the crustal correction can be compared to the Bouguer correction extending from the surface to the Moho. A choice of the reference density model basically leads only to a change of the constant level of the computed gravity anomaly, which is not considered in this study. The only important parameter is the reference density of the upper mantle. It has been demonstrated that possible differences of this parameter from the

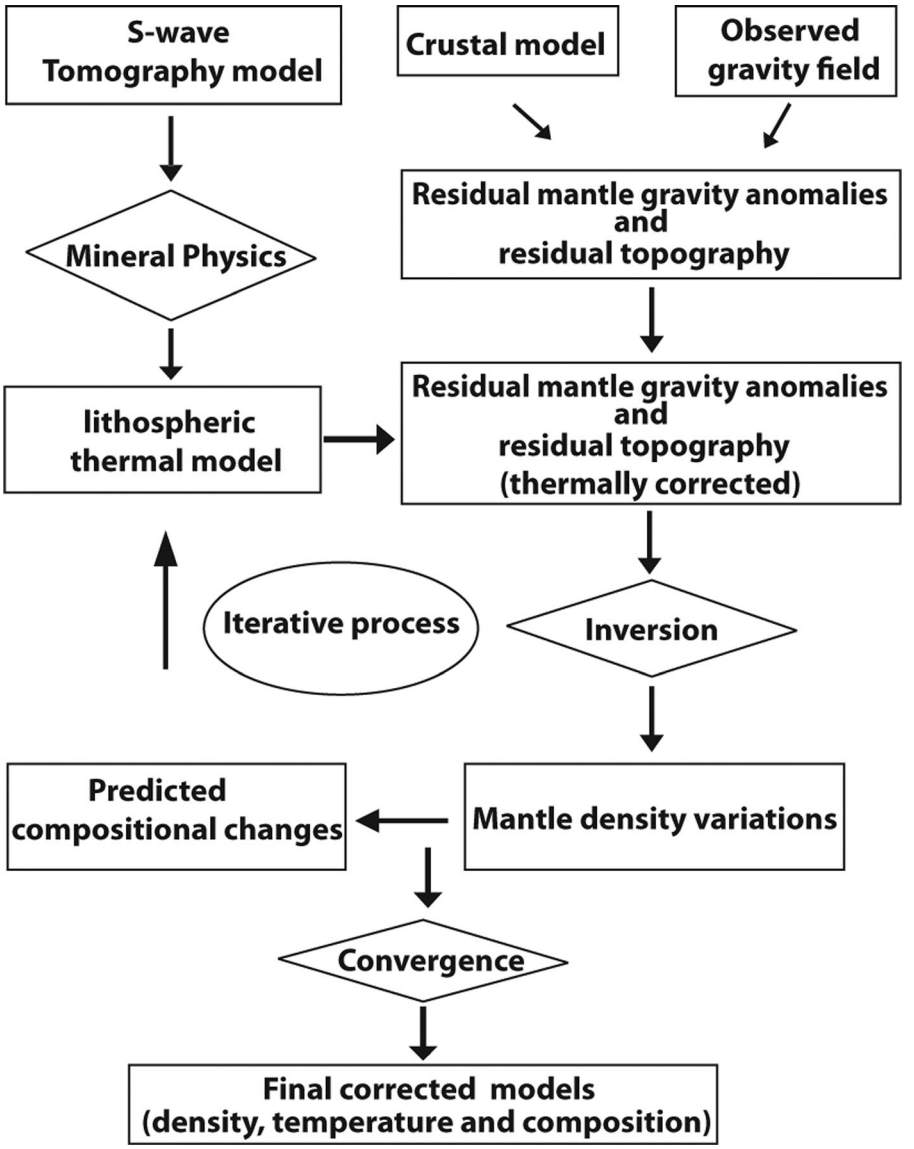

Figure 2. Workflow of the main data processing steps used in this research.

average density of the uppermost mantle do not affect the result significantly [e.g., *Mooney and Kaban*, 2010].

In this study, we use the same reference model that was used in *Mooney and Kaban* [2010] and earlier in the global study of *Kaban et al*. [2003]. It implies zero topography, a 15 km thick upper crust with density 2.7 g/cm^3 and a 25 km thick lower crust with density 2.94 g/cm^3. Average density of the uppermost mantle is set equal to 3.35 g/cm^3. This model is balanced with old (180 Ma) oceanic lithosphere according to the cooling plate model [*Kaban et al*., 1999]. Both models produce the same pressure at 40 km depth.

The gravity anomaly of each layer within the Earth's crust and mantle is calculated using 3-D algorithms for a spherical Earth, taking into account changes of density in the horizontal and vertical directions and the average elevation of each cell. The sum of the gravity influence of each volume, corresponding to the initial grids, is computed in each grid cell on the surface. We use the algorithm of *Artemjev and Kaban* [1994] which is based on the formulas of *Strakhov et al*. [1989]. The estimated accuracy of the calculations is 1 mGal. The gravity effect in each point is calculated taking into account density (or boundary) variations for the whole Earth. For these purposes, the high-resolution model of the North American crust [*Tesauro et al*.,

2014a] is embedded in the global model, which was previously used for estimation of the strength and elastic thickness of the lithosphere [*Tesauro et al*., 2012b]. The global crustal model (in this study, CRUST1.0 [*Laske et al*., 2013]) has been modified to include detailed compilations of the Moho depth and velocities in the crystalline crust in North America, Eurasia, and Australia [*Tesauro et al*., 2008; *Stolk et al*., 2013; *Collins et al*., 2003] and of the sedimentary thickness in the continents [*Tesauro et al*., 2008; *Mooney and Kaban*, 2010] and oceans [*NOAA*, 2010]. Despite the fact that the global crustal model is less reliable than the regional one for NA, it is sufficient to account for distant effects in the gravity calculations [*Kaban et al*., 2004]. By removing the crustal effect from the observed gravity we estimated the residual mantle anomalies of the gravity field.

The crustal density model is also used to estimate residual topography (t_{res}), which represents that part of the observed topography, which is under or overcompensated by the crustal structure in an isostatic sense [e.g., *Kaban et al*., 2004]:

$$t_{res} = \frac{1}{\bar{\rho}}(\rho_{top})t_{obs} + 1\bar{\rho}\int_0^M \Delta\rho(h)\left(\frac{R-h}{R}\right)^2 dh, \quad (1)$$

where, ρ_{top} is the average block density (including the effects of ice and sediments) of topography (t_{obs}); $\bar{\rho} = 2.67$ g/cm^{-3} is the average density of t_{res}; $\Delta\rho(h)$ is the density anomaly (including water) relative to a horizontally homogeneous reference model, t is the topography height (zero for sea areas), h is the depth below geoid, R is the radius of the Earth. The integration is limited to the Moho, since below this boundary $\Delta\rho(h)$ is assumed to be zero at this stage. This equation describes a local type of isostasy; therefore, the residual topography also includes all variations that differ from this type.

The residual topography is an important constraint often used in geophysical studies, e.g., in dynamic modeling [*Boschi et al*., 2010; *Faccenna and Becker*, 2010; *Ghosh et al*., 2013]. This parameter chiefly combines three factors [*Kaban et al*., 2004]. The first one relates to isostatic anomalies (associated with flexurally supported load) and the corresponding stress field in the lithosphere. These anomalies normally dominate in the short wavelengths. The long-wavelength disturbances, e.g., related to postglacial deformations, have relatively small amplitudes (up to 200 m in the extreme case), which are below computational uncertainties. The second factor relates to the lithosphere density heterogeneity below the Moho, which are not taken into account at this stage. In this way, high-density lithospheric keels of the old continental lithosphere control near-zero topography, while the low-density lithosphere pushes up the topography. The third part represents the dynamic topography associated with normal stresses at the base of the lithosphere, which are induced by mantle flow.

The main object of this study is to identify anomalous density distributions in the upper mantle. Therefore, it is necessary to suppress the impact of other factors. The local isostatic disturbances might be filtered out to some extent by considering only mid or large-scale anomalies. The dynamic part of t_{res} can be calculated from global convection models. In this study, we use one of the most recent results [*Petrunin et al*., 2013]. This global dynamic model is based on the tomography model S40rts [*Ritsema et al*., 2011] and implies 3-D viscosity distribution in the mantle. The dynamic effect is estimated for the density anomalies below 325 km. In the same way, we estimated the gravity effect of the deep mantle (also below 325 km) including dynamic perturbations. This effect is also removed from the residual mantle anomalies. Therefore, the remaining part reflects the impact of the heterogeneity of the lithospheric and sublithospheric mantle up to a depth of 325 km.

3.2. Joint Inversion of the Residual Gravity and Residual Topography

The residual mantle anomalies reflect the effect of density variations in the upper mantle induced by both thermal and compositional changes. However, construction of a reliable 3-D model based only on these anomalies is impossible since the inverse gravity problem is basically ill posed. The problem of determination of the density distribution ρ may be formulated as finding:

$$\min\{||A\rho - g_{res}||^2 + \alpha\Omega(\rho)\}, \quad (2)$$

where $\boldsymbol{A}$ is the integral operator converting density into the gravity field [*Kaban*, 2011]. The operator $\boldsymbol{A}$ has no continuous inverse $\boldsymbol{A}^{-1}$; thus, the direct solution is neither unique nor stable. To overcome this principal

weakness, a so-called regularization term Ω is added [*Tikhonov and Arsenin*, 1977], where α defines strength of regularization.

Therefore, having one parameter, namely, the gravity field, one can reliably determine only one parameter. In the study of *Mooney and Kaban* [2010], the average density of a 100 km thick layer was estimated. The density-depth relation might be prescribed a priori using some additional constraints based on petrological models [e.g., *Griffin et al*., 2003], which will be demonstrated later, but in any case a reliable solution gives only one integral parameter.

The computed t_{res} opens additional possibilities to constrain 3-D density structure of the upper mantle. Both fields (residual gravity and residual topography) are induced by density heterogeneity but essentially in a different way depending on their size and depth (M. K. Kaban et al., Cratonic roots under North America are shifted by basal drag: New evidence from gravity and geodynamic modeling, submitted to *Nature Geoscience*, 2014). The inverse problem is then reformulated [*Kaban et al*., 2013; Kaban et al., submitted manuscript, 2014]:

$$\min\{||A\rho - g_{res}||^2 + k||B\rho - t_{res}||^2 + \alpha||\rho - \rho_{ini}||^2\}, \quad (3)$$

where $\boldsymbol{B}$ is the integral operator converting densities to topography perturbations, $\boldsymbol{k} = \boldsymbol{2\pi G\rho_t}$ is the scaling coefficient normalizing topography w.r.t gravity, and the regularization condition implies that the obtained density structure should be close to a predefined model or the density perturbations should be minimum when such a model is not available ($\rho_{\boldsymbol{ini}} = 0$). The inversion is performed in a spherical harmonic domain, where the solution might be found separately for each spherical coefficient [e.g., *Forte and Peltier*, 1991]. The topography perturbations are computed for a predefined viscosity profile, which is presented by *Steinberger and Calderwood* [2006] based on global dynamic models. The numerical method is based on spherical harmonic decomposition of the initial fields [e.g., *Forte and Peltier*, 1991] with latest improvements [*Petrunin et al*., 2013].

The inversion technique has been extensively tested. A test density structure that is representative of the real Earth has been implemented in a spherical shell and its effect on the gravity field and topography has been computed. Some noise has been added and the resulting fields have been inverted to reproduce density structure. It has been demonstrated that in most cases it is possible to reconstruct initial density patterns including various combinations of positive and negative anomalies [*Kaban et al*., 2013; Kaban et al., submitted manuscript, 2014]. In particularly, various types of the dipole anomalies (for both, vertical and horizontal positions of the positive and negative anomalies) are well recognized. The geometry of inclined bodies (like subducting slabs) is well recovered. Significantly it is possible to estimate the depth of anomalies, e.g., in the uppermost mantle versus the midcrust. The most challenging case for the inversion is for anomalies of the same sign; in the inversion they are merged into one smeared anomaly (Kaban et al., submitted manuscript, 2014). It is also proven in this study that the results do not depend substantially on a precise choice of the damping factor.

The amplitude of the inverted densities is reduced due to the regularization damping, similar to tomography models. The amplitude might be up to 30–50% less than the amplitude of the initial anomaly; however, the anomaly pattern may be smeared. Therefore, this method is more accurate regarding the shape and location of the anomaly rather than its amplitude. This fact should be taken into account during the interpretation.

4. Initial Data

4.1. Initial Gravity Field

The initial gravity model (EIGEN-6c2) is based on a combination of satellite and terrestrial data [*Förste et al*., 2011]. The field is completed up to 1949 spherical harmonic degree/order. The Bouguer gravity anomalies have been computed by removing the effect of topography/bathymetry and ice from the observed gravity field (Figure 3). We use the ETOPO-1 model compiled by NOAA (www.ngdc.noaa.gov/mgg/global/global.html). The sum of the gravity influence of each volume corresponding to the initial grids is computed in each grid cell on the surface taking into account the average elevation (or depth) and considering all spherical effects [*Kaban et al*., 2004]. The density of topography and sea water is considered to be equal to 2.67 and 1.03 g/cm^3, respectively.

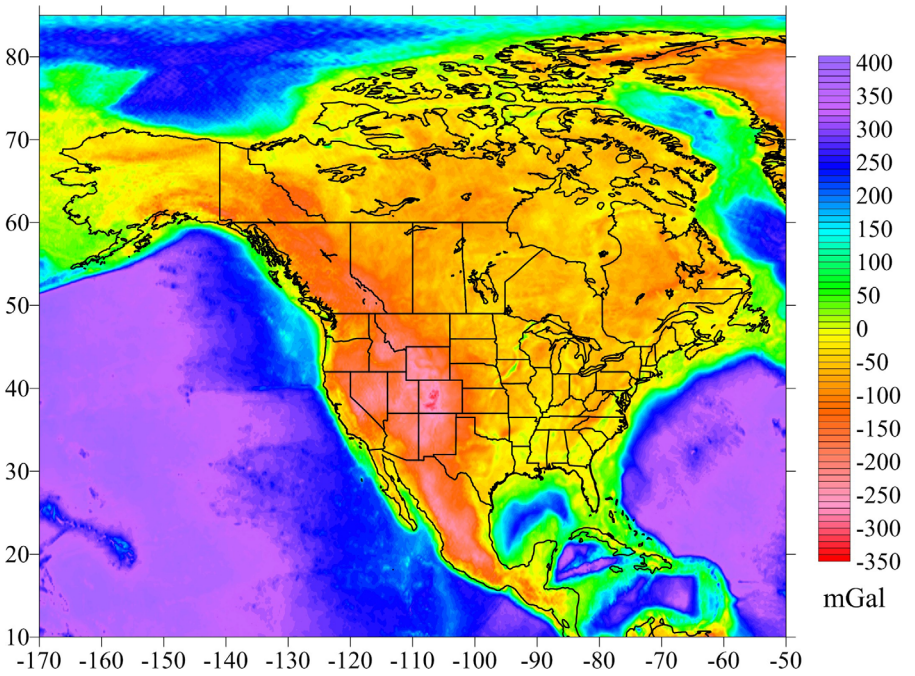

Figure 3. Bouguer gravity anomalies of the gravity field (see text for further explanation).

4.2. Crustal Model

NACr14, the new 3-D model of the NA crystalline crust [*Tesauro et al.*, 2014a] used in this study, has a resolution of 1° × 1° and provides depth and average velocity of the main layers: upper, middle, and lower crust (Figures 4a–4c). It is based on the most complete database of available seismic data in this region, primarily reflection and refraction profiles and receiver function data (USGS database) [*Mooney*, 2014]. In the areas not covered by the database, *P* wave seismic velocities and thickness of the crustal layers have been estimated on the base of a statistical analysis for each predefined geological province. The upper and lower boundaries of the crystalline crust have been taken according to the model of *Mooney and Kaban* [2010]. The sediment thickness map of these authors has been improved in the offshore regions using the new compilation of NOAA [2010]. The density of sediments was estimated by *Mooney and Kaban* [2010] by defining smoothed density-depth functions that characterize each type of sedimentary basin (from soft to hard).

The new NA crustal model shows the main variations of the crustal structure reflecting the tectonic evolution of the continent. The thickness of each crustal layer reaches maximum values up to ∼20 km, but on average is between 11 and 13 km (Figures 4a–4c). To estimate the gravity effect of the crystalline crust, we converted the average velocity of each layer in density (Figures 4d–4f), using the equations provided by *Christensen and Mooney* [1995]. Velocities and thus densities of the lower crust vary in a larger range than those of the other layers, on account of the presence of a 7.0× layer (i.e., Vp > 7.0 km/s) in the lowermost part of the crust of some Archean and Proterozoic regions. The crystalline crust in the Gulf of Mexico consists of only one layer (presumably basaltic in composition), with an average density of ∼2.90 g/cm^3.

4.3. Tomography Models

We use seismic velocity variations in the upper mantle to estimate the temperature distribution as constrained by mineral physics equations [e.g., *Stixrude and Lithgow-Bertelloni*, 2005]. The S-velocity structure of the NA mantle has been recently modeled on regional [*Marone et al.*, 2007; *Nettles and Dziewonski*, 2008; *Bedle and van der Lee*, 2009; *Yuan et al.*, 2011] and global scale [e.g., *Ritsema et al.*, 2011; *Schaeffer and Lebedev*, 2013] by surface waves inversion. The models used in this study are displayed in Figures 5a and 5b in terms of absolute velocities at a depth of 100 km and along one cross section. They consistently show principal (large-scale) patterns, but they are quite different in detail, likely because they are derived from both different data and inversion techniques, e.g., in regularization parameters such as damping. In particular, as already observed in previous studies [e.g., *Becker*, 2012], the amplitude of the anomalies

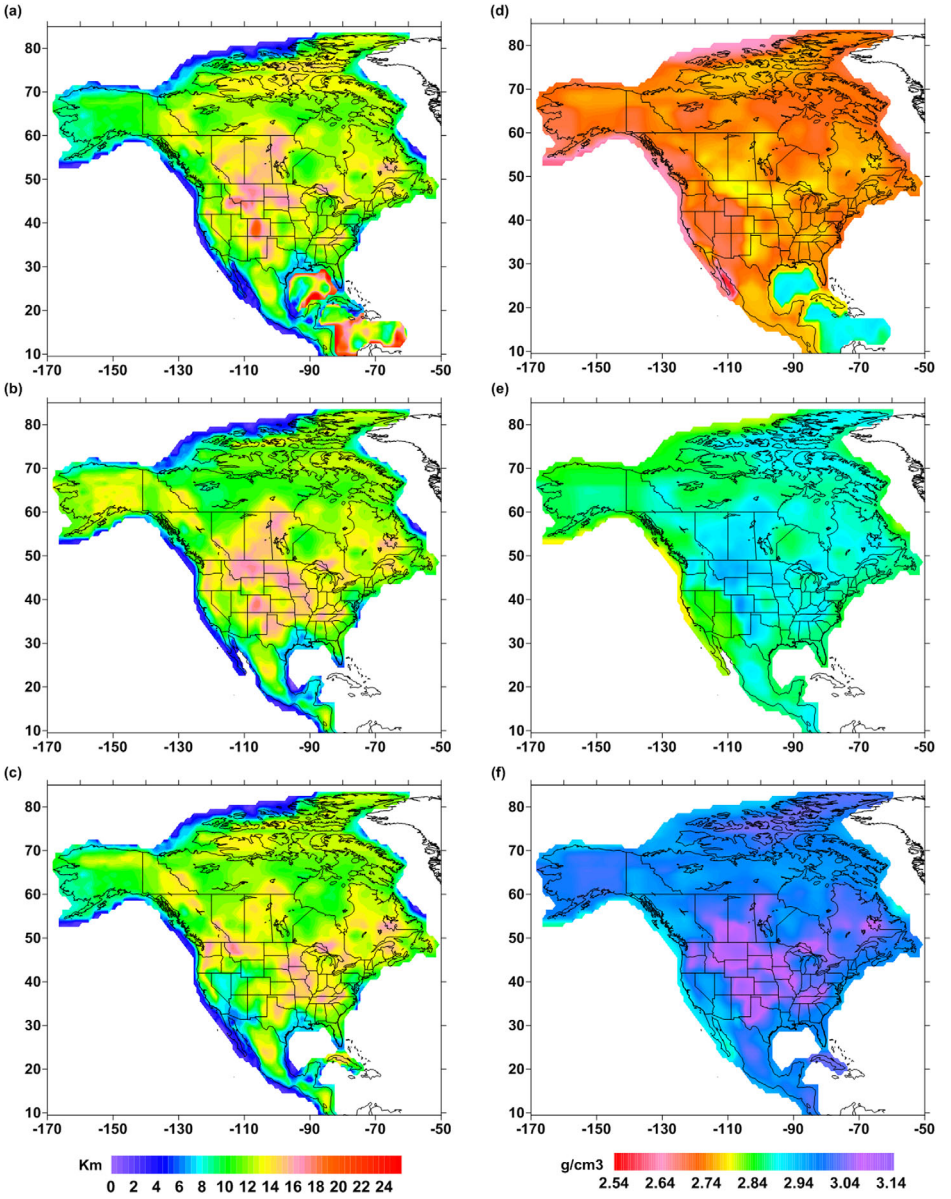

Figure 4. The 3-D model of the crystalline crust of the NA continent; (a–c) thickness of the upper, middle and lower crust, respectively; (d–f) density of the upper, middle and lower crust, respectively. The crystalline crust in the Gulf of Mexico has no internal division and its density corresponds to the entire crystalline crust. The crystalline crust of Cuba Island and the Gulf of California is divided in two layers and their densities and thickness refer to the upper and lower layer.

may largely vary among different tomographic models. The uncertainty of tomographic models strongly affects their interpretation with respect to compositional and thermal properties. To estimate the thermal and compositional structure of North America, we selected two tomography models derived from similar data. In making this choice, we first selected one of the most recent regional tomography models (NA07) [*Bedle and van der Lee*, 2009], which in comparison with some others [e.g., *Nettles and Dziewonski*, 2008; *Yuan et al*., 2011] uses a smoother reference velocity model, thus providing more reliable values of absolute velocities.

Bedle and van der Lee [2009] fit regional *S* and Rayleigh wave trains generated by the earthquakes around North America that occurred between the years 2000 through 2006, including waveforms from the Transportable Array stations of the EarthScope's USArray. They implemented a 3-D *S* wave velocity model of the upper mantle beneath North America from a suite of best fit models, each created using different parameterization

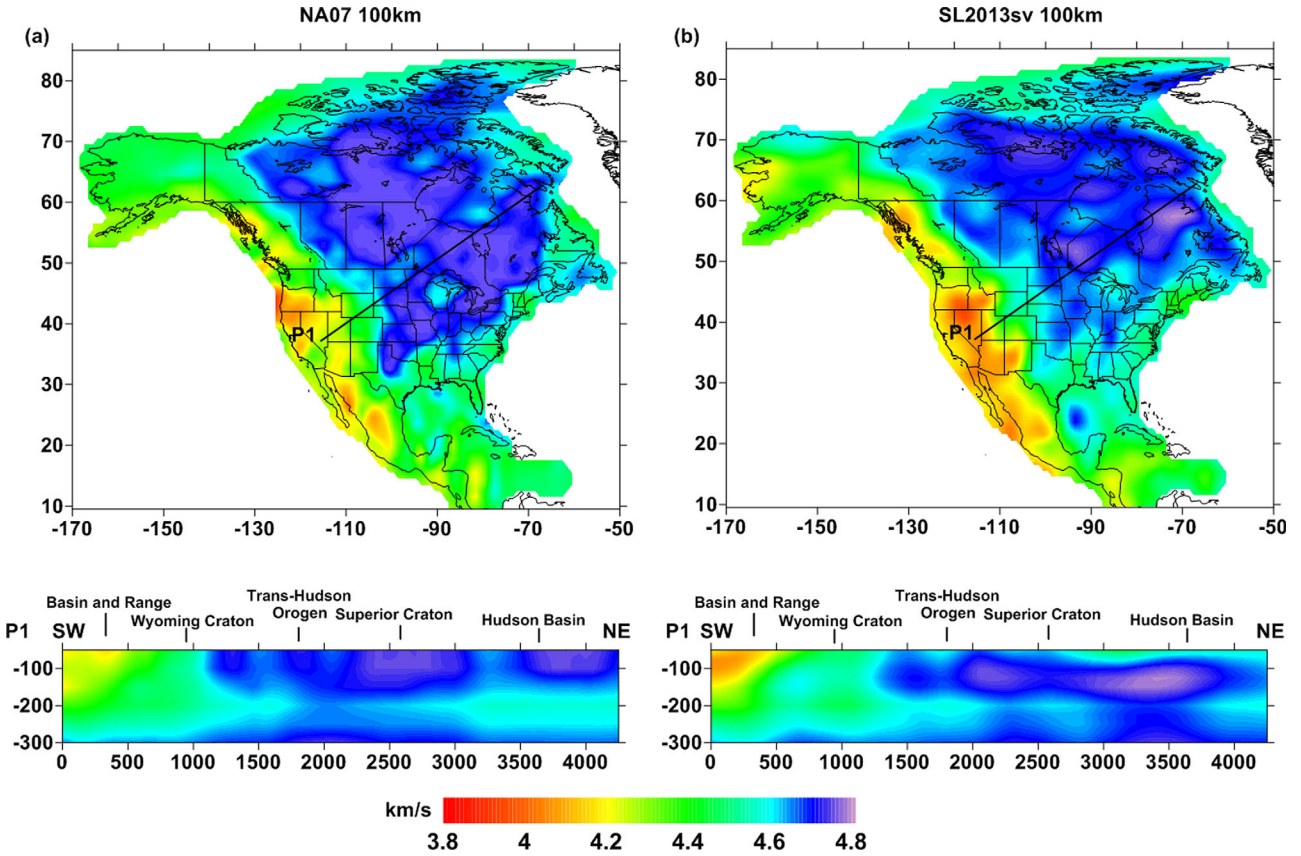

Figure 5. *S* wave velocity (km/s) at a depth of 100 km provided by (a) the regional tomography model NA07 [*Bedle and van der Lee*, 2009] and (b) the global tomography model SL2013sv [*Schaeffer and Lebedev*, 2013].

and data subset. This model was derived relative to a 1-D reference model, MC35 [*van der Lee and Nolet*, 1997], which is based on PREM-C [*Dziewonski et al.*, 1975]. The tomography model was also corrected a priori for crustal heterogeneities, using the same seismic constraints employed in the NA04 model [*van der Lee and Frederiksen*, 2005], as well as the midcontinent data introduced in the model IL05 [*Bedle and van der Lee*, 2006].

The second model we have selected (SL2013sv) [*Schaeffer and Lebedev*, 2013] is the most recent global S-wave model (vertically polarized), obtained with similar data and technique employed in NA07. In this way, the possibility of a disagreement between the two models, related to the different assumptions used, was strongly reduced. In fact, as NA07, SL2013sv was developed using the partitioned waveform inversion technique [*Nolet*, 1990] and benefited from the stations provided by the USArray. The model was derived relative to a 3-D reference model of the crust (CRUST 2.0) [*Bassin et al.*, 2000] and 1-D model of the mantle (AK135) [*Kennett et al.*, 1995]. It should be noted that neither model, mainly based on the vertically polarized shear waves, takes into account the effect of anisotropy. Seismic anisotropy will bias isotropic velocity estimates, and consequently the temperature estimates, particularly in the regions where seismic sampling is dominated by one propagation or polarization direction [e.g., *Yuan et al.*, 2011].

Both models show the well-known division of the NA continent between western and the eastern North America which are characterized by low and high upper mantle velocities, respectively (Figures 5a and 5b). As also observed in previous models [e.g., *van der Lee and Nolet*, 1997], such a sharp boundary is marked by a range in shear velocity of nearly 10% at a depth of 100 km, which corresponds to a thermal contrast of ~500°C, without considering the effect of compositional variations [*Goes and van der Lee*, 2002]. The highest cratonic velocities are found primarily beneath the largest craton of North America, the Superior craton, which also has the deepest mantle root as inferred from the seismic model. In particular, in the northeastern part of the Superior craton the velocities from the SL2013sv at a depth of 100 km are 0.05 km/s faster than those of NA07 model (Figures 5a and 5b). In both models, the lithosphere beneath the cratons extends to

an average depth of ~200 km, but can reach locally a depth of 250 km, as observed in the previous study of *Yuan et al*. [2011] that estimated the depth of this boundary from changes in the direction of azimuthal anisotropy. In contrast, the Archean Wyoming craton has significantly lower average velocity in the upper 200 km in comparison with other Archean and Proterozoic provinces. Another large-scale seismic anomaly observed in both models is the low-velocity zone that underlies most of the western margin of the continent and which extends to the eastern boundary of the Rocky Mountain Cordillera. This zone extends from southern Alaska in the north to the south until the Pliocene-Quaternary Trans-Mexican Volcanic Belt. The lowest measured velocities underlay the Gulf of California and extend northward beneath the Salton Trough in South California, the Snake River Plain volcanic belt and the Basin and Range province, down to a depth of ~150 km.

In the southern part of the continent, the low velocities in SL2013sv extend more to the east, including part of the Colorado Plateau. The western margin remains distinct from continental North America down to ~200 km. Within the areas offshore, SL2013sv identifies in the western part of the Gulf of Mexico a small region characterized by fast velocities that is absent in NA07. In terms of depth-dependence (see cross sections in Figures 5a and 5b), the main difference between the two models occurs in the shallower mantle (at a depth $<$75 km), where NA07 shows significantly faster velocities than SL2013sv and the correlation coefficient is lower (~0.8) than in the deeper layers (~0.9 at a depth of 100–150 km). This difference is reduced beneath the western margin (~0.10 km/s) with respect to the cratons, where it reaches ~0.15 km/s. This kind of discrepancy is also observed in the uppermost mantle in other tomographic models [*Becker*, 2012] and might be related to the differences in the crustal correction. In fact, the effect of the crust might not be fully removed from SL2013sv because the crustal model (CRUST 2.0) [*Bassin et al*., 2000] is remarkably different from the actual seismic data [*Tesauro et al*., 2014a].

Therefore, we can conclude that the differences between the two models are typical of the whole family of seismic tomography models that have been constructed up to now. They are quite similar on a regional scale but show some remarkable differences in local details, especially in the uppermost mantle. Therefore, conversion of these seismic models into temperature variations introduces uncertainties that are usually not specified explicitly.

5. Residual Mantle Gravity Anomalies and Residual Topography

After constructing the crustal model, we calculate its gravity effect, as previously discussed, relative to a horizontally layered reference model. Our goal is to correct for the gravitational effect of the laterally varying crust by replacing it with the homogeneous reference crustal model. We thereby obtain the residual, or mantle gravity field. The topography/bathymetry correction has been already included in the Bouguer anomalies. First, we calculate the gravity effect of low-density sediments (Figure 6a). This field is negative relative to the standard density of the upper crust (2.7 g/cm^3) and varies from $-$140 to 0 mGal. The largest minima are located over the Gulf of Mexico and near the northern and the eastern continental margin, on account of the thick ($>$10 km) and low-density (2.5 g/cm^3 on the average) sedimentary layer. On the other hand, the older basins (e.g., Michigan and Illinois) are characterized by negligible anomalies. In fact, despite the remarkable depth of these basins ($>$5 km), the high density of their sedimentary infill (2.65 g/cm^3) is close to that of the reference model [*Mooney and Kaban*, 2010].

In the same way, we compute the gravity effect of the density variations within the crystalline crust (Figure 6b). This field depends on both density and thickness of the crystalline crust (Figures 4a–4f). The largest positive anomalies ($>$150 mGal) correspond to regions with high-density lower crust ($>$3.0 g/cm^3) (Figure 6c), as beneath the Superior craton and the Rocky Mountains, close to the Montana-Canada border. Strong negative anomalies ($<-$50 mGal) are estimated in the regions characterized by crustal thinning, like those along the southeastern Atlantic margin and having anomalous low crustal densities, such as the Basin and Range province, on account of the absence of a high-velocity lower crust [*Tesauro et al*., 2014a].

The most significant gravity effect is generated by lateral variations in the Moho depth (Figure 6c). Within the continent, the gravity effect is mostly in the range $\pm$150 mGal with the maximum over the old regions characterized by high crustal thickness. The largest positive anomalies ($>$300 mGal) are located in the oceanic regions that have very thin crust ($<$15 km).

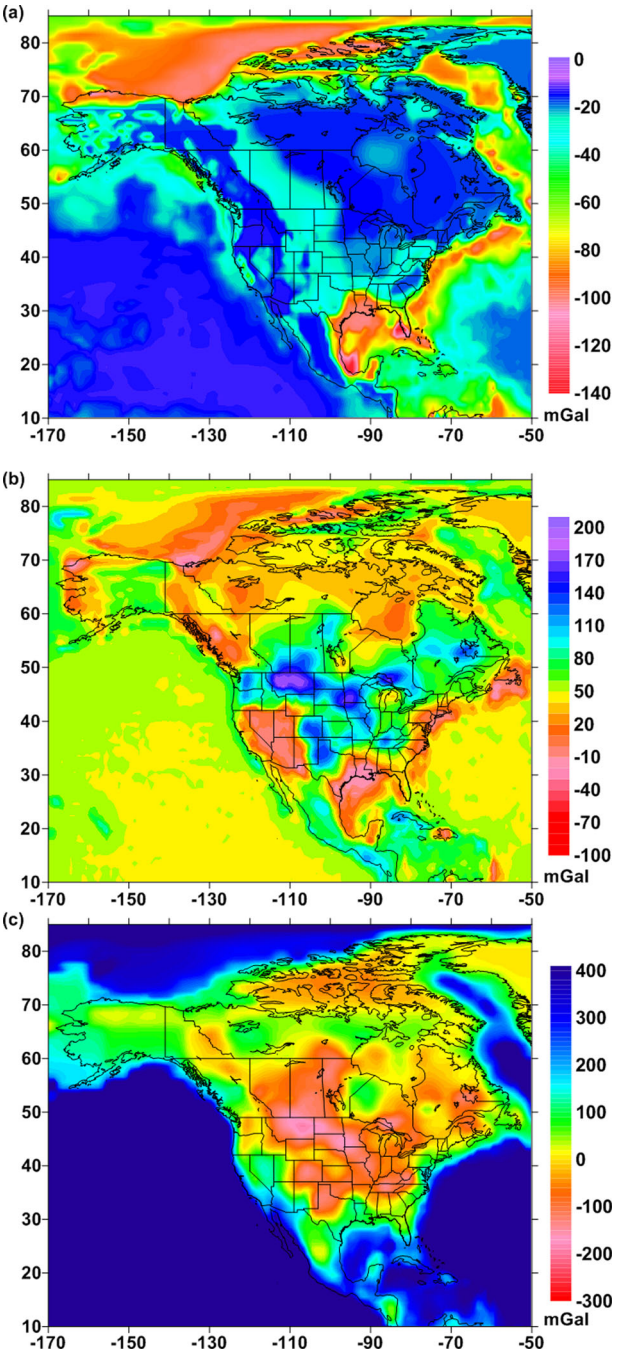

Figure 6. Anomalous gravity effect of the crustal layers: (a) sediments (as contrasted to an assumed density 2.7 g/cm^3 for crystalline crust); (b) crystalline crust; (c) Moho. Density of the lower crust and uppermost mantle is set to 2.94 and to 3.35 g/cm^3, respectively, according to the reference model. Additional positive effect is created where the Moho is shallower than 15 km, corresponding to lower boundary of the upper layer of the reference model (see text for further explanation).

Removal of the total gravity effect of the crust from the observed gravity field yields the residual upper mantle gravity anomaly map (Figure 7a). In addition, the effect of deep density heterogeneities located below 325 km is removed from the gravity field (see section 3.1). The residual field is slightly filtered to remove artifacts related to errors in the initial crustal model and the effect of local isostatic disturbances. A Gaussian filter with $\lambda > 250$ km (half amplitude) is applied on the sphere. The mean value of this field is not interpretable and set to zero, since it depends on a choice of the reference model and on distribution of the anomalous masses over the whole Earth (e.g., the total effect of the oceanic water and topography is strongly negative everywhere). Variations of the residual anomalies are mostly within $\pm$330 mGal and reflect density changes in the upper mantle induced by both thermal and compositional heterogeneities.

Following *Mooney and Kaban* [2010], we summarize the uncertainties related to the crustal correction. The following factors contribute to the overall error of the residual gravity anomalies and residual topography: (1) the measured gravity; (2) the density model of sediments; (3) densities of the crystalline crust; and (4) uncertainty of the Moho position. The initial gravity field model is very accurate for North America and its uncertainty is insignificant compared to other factors. The density of sediments is basically the same as used by *Mooney and Kaban* [2010]. They estimate the corresponding error in the gravity field as 10–12 mGal for relatively large structures, which correspond to the resolution of this study (1° × 1°).

The uncertainty of the crystalline crust density is based on estimations of *Christensen and Mooney* [1995], who gives a value of $\pm$0.05 g/cm^3 for an individual layer. Since the crystalline crust in our model combines three independent layers, the total uncertainty of the average density may be reduced to $\pm$0.03 g/cm^3. Thus, the contribution of the crystalline crust depends on its thickness and may reach 25–50 mGal. The Moho model is

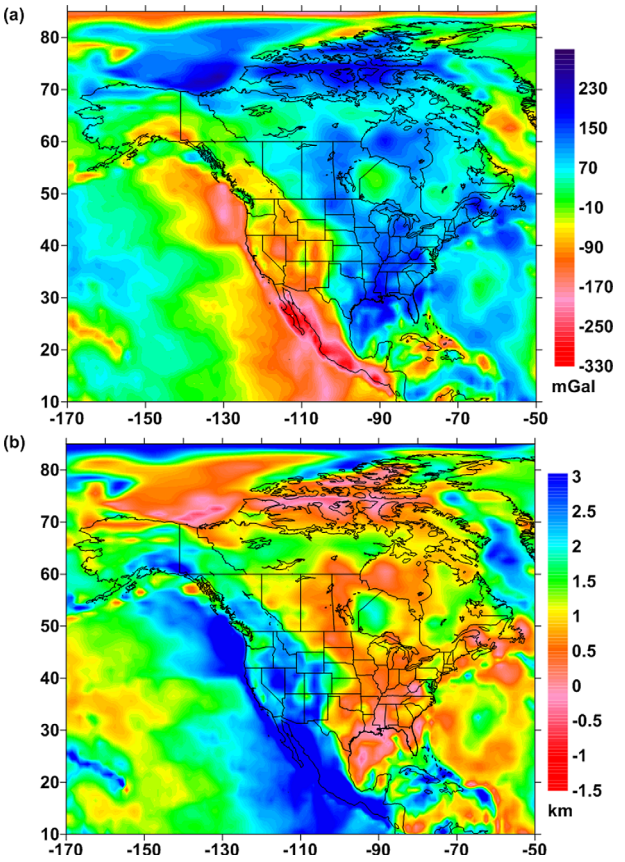

Figure 7. (a and b) Residual mantle gravity anomalies obtained after removal of the crustal gravity effect from the observed field (see text for further explanations). The average level is set to zero for the study area. (b) Residual topography (t_{res}): the part of topography, which is noncompensated or overcompensated by the crustal structure. Zero level corresponds to the reference density model (see text for further explanations).

again the same as in *Mooney and Kaban* [2010], who estimate corresponding gravity errors from 30 mGal for well-studied regions to 60 mGal for the areas with thick crust and poor observation covered.

Combining all error sources and considering them independent, the estimated standard deviation in the mantle gravity anomaly map varies from 40 mGal for the well-studied regions of North America with thin (<35 km) crystalline crust, to about 75 mGal, for the regions with thick (>35 km) crust and poor seismic coverage [*Mooney and Kaban*, 2010]. The corresponding error in the residual topography varies from 0.35 to 0.65 km correspondingly.

The most prominent feature of the residual mantle field is the difference between the older, stable central and eastern regions and the younger, active Mesozoic-Cenozoic provinces of the western margin. Generally, this result agrees with those obtained by *Mooney and Kaban* [2010] based on their previous crustal model. However, we observe also some regional differences due to changes in the initial crustal model. For example, the positive anomalies are remarkably lower (<150 mGal) in some regions (e.g., over the Canadian Shield) than in the previous study.

The largest negative anomalies (<−100 mGal) are found in the southwestern U.S. (Basin and Range), Mexico, and Gulf of California. These minima correspond to low Pn values (<7.9 km/s) [*Tesauro et al*., 2014a] and low upper mantle velocities [e.g., *Bedle and van der Lee*, 2009; *Shen et al*., 2013], which supports a thermal origin [*Goes and van der Lee*, 2002]. Beneath the Proterozoic and Archean terranes the gravity anomalies are positive and on average relatively high (>100 mGal), thereby showing a good correlation with the positive seismic velocity anomalies in the upper mantle [e.g., *Nettles and Dziewonski*, 2008; *Bedle and van der Lee*, 2009; *Yuan et al*., 2011]. Therefore, these features provide clear evidence for a thick and cold lithosphere. However, beneath these regions the gravity anomalies are heterogeneously distributed and are not strongly correlated with the age of the geological provinces. We notice that slightly positive values (∼50 mGal) correspond to the Canadian Proterozoic platform and to the northwestern part of the Archean Superior craton, while stronger anomalies (>150 mGal) are found beneath the Proterozoic Trans-Hudson Orogen.

However, in some off-craton regions, the correlation between the seismic and gravity anomalies becomes much weaker. In fact, beneath the northern margin, the Grenville province, the southwestern part of the Appalachian, and the Gulf of Mexico the gravity anomalies are positive (∼150 mGal or even larger) similar to those observed beneath the interior part of the continent. However, these regions are characterized by high average *Pn* values (8.0–8.1 km/s) and zero or very weak (either positive or negative) seismic velocity anomalies [e.g., *Nettles and Dziewonski*, 2008; *Bedle and van der Lee*, 2009; *Yuan et al*., 2011]. These findings support the hypothesis that temperature is not the only factor controlling density structure of the mantle, but compositional variations exist as well.

The t_{res}, computed from the same crustal model (Figure 7b), is controlled by the same factors as the residual gravity, although in a different way (see section 3.1). The t_{res} is also filtered to remove small-scale artifacts and the dynamic contribution from the anomalous masses below 325 km is removed as well. Potential uncertainties of the t_{res} are due to the same factors as for the residual mantle gravity anomalies. They may reach $\pm$0.3 km for the well-studied continental regions with thin ($<$35 km) crystalline crust and up to $\sim$0.55–0.6 km for the regions with thick ($>$35 km) crust and poor seismic coverage. Previously, the residual topography was estimated for western North America [e.g., *Becker et al*., 2014] and also for the entire continent [e.g., *Ghosh et al*., 2013]. It is clear that the different crustal models strongly affect the results [e.g., *Ghosh et al*., 2013], preventing us from making a quantitative comparison. Furthermore, in previous works, the reference crustal density models are different, which results in a shift of the t_{res}, and the contribution of the deep mantle ($>$325 km) is included.

In contrast with the residual gravity anomalies, western North America is mainly characterized by positive t_{res} (up to $\sim$4 km) and the central and eastern parts of the continent by negligible ($\pm$0.5 km) or weakly negative t_{res} (mostly >-1 km; Figure 7b). However, as for the residual gravity, such a difference is more evident in the southern part of the continent. Although the t_{res} is usually not correlated with topography, we can observe that in this case there is a good correspondence between the high elevation characterizing the western margin of the NA continent and part of its interior (e.g., the Rocky Mountains) and the positive values of the t_{res} ($>$2 km). This means that the uplifted topography of western North America is largely supported by the low-density upper mantle, both within and under the lithosphere.

The relation between the large-scale uplift of the NA Cordillera and mantle upwelling has recently been investigated [e.g., *Hyndman and Currie*, 2011; *Becker et al*., 2014; *Ghosh et al*., 2013]. The uplift might be related to a hot back arc [e.g., *Hyndman and Currie*, 2011] and/or to an uprising mantle plume (e.g., in Yellowstone) [*Parsons et al*., 1994]. Within the western Cordillera, the anomalous topography of the Colorado Plateau (Figure 1), accompanied by recent volcanism [e.g., *McQuarrie and Oskin*, 2010], has been explained by small-scale convection and delamination processes [e.g., *van Wijk et al*., 2010; *Levander et al*., 2011] or by deep mantle flow [e.g., *Moucha et al*., 2009]. In our t_{res} map (Figure 7b), we can clearly distinguish the core of this tectonic feature, which is characterized by positive values ($\sim$1.5 km), but substantially lower than those observed in its southern and western edge and in the adjacent Basin and Ranges ($>$3 km). We conclude that the contribution of the upper mantle in this region, although it might have been important in the past [*Liu and Gurnis*, 2010] is currently weaker compared to that of the surrounding regions. This finding also supports the hypothesis that small-scale convection is currently removing the lithospheric mantle from the edge of the Colorado Plateau, causing uplift of its margins [e.g., *van Wijk et al*., 2010].

The study of *Becker et al*. [2014] has estimated negative t_{res} values along the Sierra Nevada and Cascades, interpreted as the effect of downwelling forces exerted by the ongoing subduction of Juan de Fuca plate. In contrast, our t_{res} values are positive in these regions, but not so pronounced (1.5–2 km) as in the Basin and Range ($>$3 km). We should consider that these areas are characterized by low seismic velocities [*Bedle and van der Lee*, 2009; *Yuan et al*., 2011], implying the presence of a hot upper mantle, which will provide buoyancy and hence uplifted topography. Therefore, the reduced t_{res} in respect to that of the Basin and Range might also reflect a partly counteracting downwelling effect of the subducting plate. In this case, the difference between our results and previous findings might be mainly attributed to the differences in the initial crustal model, and/or a deeper origin ($>$325 km) of the downwelling force.

Comparison of the t_{res} with the residual gravity anomalies shows that the previously determined inverse correlation between the two, such as found in Europe [*Kaban et al*., 2010] is present only beneath the tectonically active western regions. These areas have large negative anomalies (<-150 mGal) that are undercompensated by the crust, being characterized by t_{res} of about $+3$ km. In contrast, most of the regions of the eastern and central part of North America have large positive mantle gravity anomalies ($>$150 mGal) and are characterized by negligible values of t_{res} ($\pm$0.5 km). Contrary to the residual gravity, the zero level of t_{res} is strongly related to the reference crustal density model. Therefore, the crust of central and eastern North America is almost compensated with respect to the 40 km thick reference model. Two exceptions are the Canadian Proterozoic platform and the northwestern part of the Superior craton that is characterized by weak positive gravity anomalies and positive t_{res} (up to 2 km). These findings indicate that the lithospheric mantle density is not so high as might be expected from the fast velocities detected in the tomographic

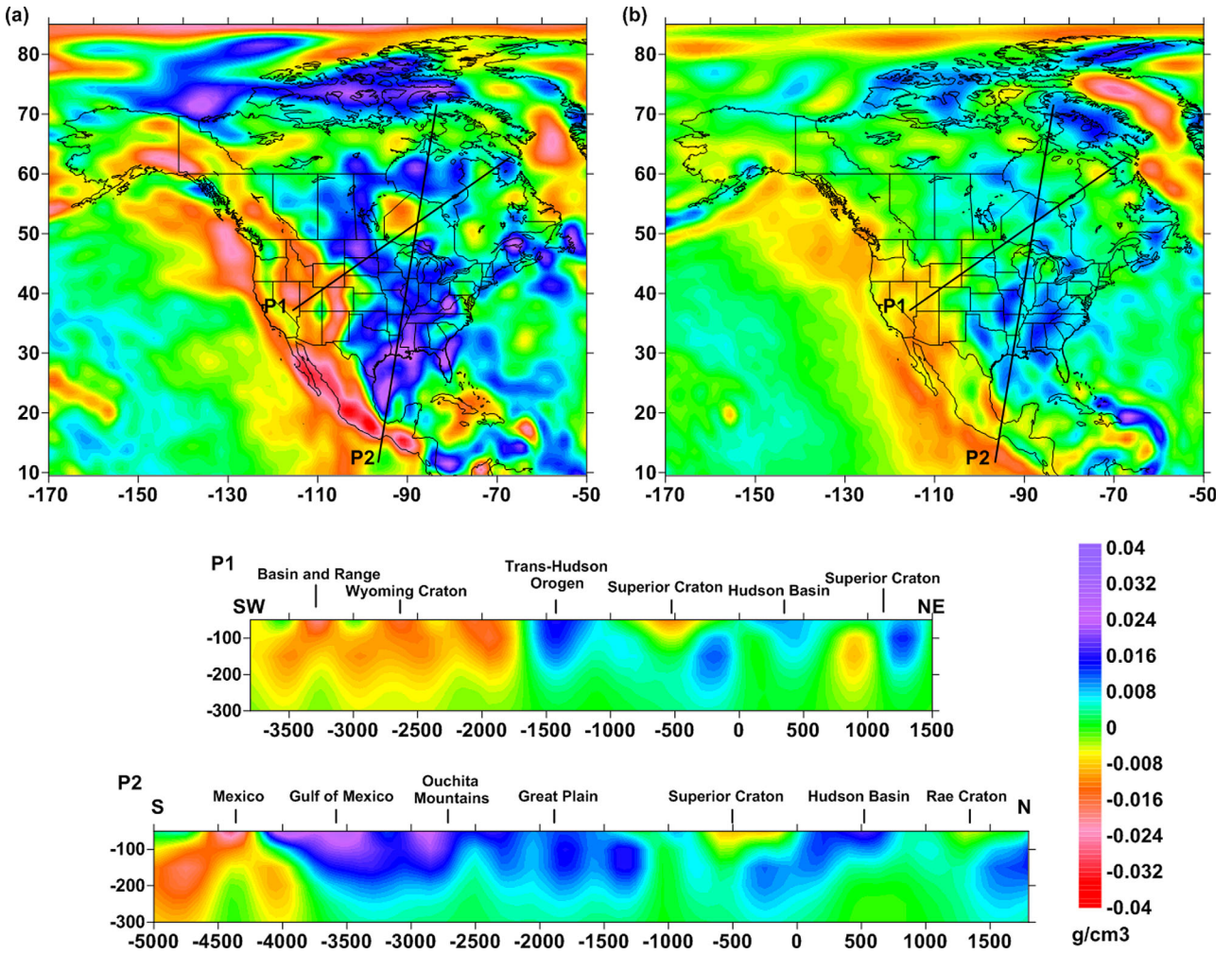

Figure 8. Two slices of the density model of the mantle based on the joint inversion of the residual mantle gravity anomalies and residual topography. (a) Density anomalies at a depth of 100 km; (b) density anomalies at a depth of 200 km. Black lines show the location of the two vertical cross sections displayed at the bottom (see text for further explanations).

models [e.g., *Nettles and Dziewonski*, 2008; *Bedle and van der Lee*, 2009; *Yuan e al*., 2011]. These results provide evidence for a buoyant upper mantle, possibly because of its chemical depletion in garnet (Gt) and iron.

6. Three-Dimensional Density Model of the Mantle

The residual gravity field and residual topography have been inverted to assess the 3-D density distribution of the NA upper mantle (see section 3.2). The inversion has been performed for seven layers centered at depths of 15, 50, 100, 150, 200, 250, and 300 km. The uppermost layer (15 km) retains errors within the assumed crustal model, while the other layers represent density variations in the upper mantle. Two slices through the density model corresponding to the depth of 100 and 200 km are shown in Figures 8a and 8b, together with two cross sections. The observed density anomalies, varying within the range ± 0.04 g/cm^3, are induced by both temperature and compositional variations.

The density anomalies variation at a depth of 100 km (Figure 8a) shows a very heterogeneous distribution, similar to that of the residual mantle gravity anomalies and t_{res}, indicating that the thermal and compositional variations located in the uppermost mantle are the main factor controlling these fields. Also in this case, we can observe the division between the western region and the other part of the continent, corresponding to negative and positive density anomalies, respectively. The strongest negative anomalies (< -0.03 g/cm^3) are estimated along the Mesozoic-Cenozoic western NA margin, reflecting the presence of a warm and likely wet upper mantle. In this area we can distinguish several minima located over the

southeastern margin of Alaska, the Basin and Range Province, Gulf of California, and Baja Peninsula, all of which indicates that the upper mantle is significantly warmer beneath those regions. In contrast, the uppermost mantle is not buoyant in some other parts of western U.S., such as the inner part of the Colorado plateau and the Cascadia region, where very weak positive density anomalies are estimated. Therefore, in these regions, the possible effect of high temperatures in the mantle [*Goes and van der Lee*, 2002] should be balanced by the presence of cold, likely eclogitized, subducting lithosphere (e.g., below Cascadia).

Significant positive anomalies ($>$0.02 g/cm^3) are found in most of the Proterozoic regions, such as the Trans-Hudson Orogen, the Yavapai-Maztzal province, and the southwestern part of the Grenville province. Previous studies of the Proterozoic subcontinental lithospheric mantle (SLCM), based on interpretation of xenolith data [e.g., *Griffin et al*., 2003], estimate an average density of 3.34 g/cm^3 at a depth of $\sim$100 km and a temperature of $\sim$700°C, corresponding to an upper mantle partly depleted in high-density elements (*Fe*) and mineral phases (Gt). This value is significantly larger than that of the Archean SCLM (3.31 g/cm^3), but also significantly lower than that of the Phanerozoic SCLM (3.37 g/cm^3). In addition, temperatures of the Proterozoic upper mantle are also characterized by intermediate values between those of the Archean and Phanerozoic upper mantle [e.g., *Griffin et al*., 2004]. Therefore, the positive density variations in these regions might be interpreted as a sum of the effects of the relatively low temperatures and weak depletion or refertilization of the upper mantle by metasomatic changes (e.g., the addition of *Fe* and/or Gt). Obviously, the weight of each contribution cannot be quantified only analyzing the total density anomalies.

The pattern of positive anomalies extends farther to the south in the younger southern NA margin and in the Gulf of Mexico. In these regions, the seismic tomography does not show any remarkable velocity anomaly [e.g., *Bedle and van der Lee*, 2009]. Therefore, the source of these anomalies must be related to the presence of a high-density body that is seismically less distinguishable from peridotite rocks, such as eclogite [*Mooney and Kaban*, 2010] and/or metasomatic changes influencing more strongly density than seismic velocities. Other areas showing high positive values correspond to the northern NA margin. However, the results in the northernmost part of the study area remain questionable, since they are poorly constrained (both in the initial crustal model and seismic tomography).

In contrast, other old continental areas, such as the Archean Superior craton, the northern part of the Churchill craton, and the Proterozoic Canadian platform are mostly characterized by near-zero density variations (within $\pm$0.005 g/cm^3), suggesting that the effect of the composition and temperature in this case counteract each other. We can notice that the effect induced by a depleted mantle prevails in the northwestern part of the Superior craton where a broad negative anomaly ($\sim-$0.013 g/cm^3) is observed. On the other hand, the positive anomalies ($\sim$0.018 g/cm^3) characterizing the southern part of the Churchill craton suggest that the thermal and compositional anomalies are not balanced (Figure 8a).

At a depth of 200 km, the density distribution is quite different from that at 100 km (Figure 8b), indicating that the upper mantle is vertically, as well as laterally heterogeneous. We can observe that the differences (about $\pm$0.012 g/cm^3) between the western and the central and eastern part of the continent persist only as far north as Canada, while for the most part the mantle beneath Canada is more uniform (density variations within $\pm$0.005 g/cm^3). Negative density anomalies at a depth of 200 km are mainly located beneath the western U.S. and in the northern part of Mexico, indicating that mantle buoyancy persists to this depth. The large positive anomalies, characterizing the uppermost mantle of most of the Proterozoic terranes and the Gulf of Mexico, are also remarkably low, indicating that the high-density body is observed only in the shallowest part of the mantle. On the other hand, the broad negative density anomaly found at a depth of 100 km in the northwestern part of the Superior craton is replaced by a weak positive anomaly, suggesting a change in composition, possibly due to lithospheric fertilization, a process usually occurring in the cratonic mantle at depths $>$150 km [e.g., *Griffin et al*., 2004].

Looking at the cross sections, we can observe that the density variations ($<$0.005 g/cm^3) tend to fade below 250 km in the regions characterized by positive values (e.g., the cratons), while in the areas characterized by negative values (e.g., Basin and Range and Mexico) their amplitude ($-$0.01 g/cm^3) remains remarkable below this depth and consequently below the lithosphere, which is thin in this region [e.g., *Yuan et al*.,

2011]. Therefore, the positive anomalies are mostly located within the lithosphere, while the negative ones extend deeper in the upper mantle.

Analysis of these results indicates that we need additional data to understand the physical nature of the upper mantle density heterogeneity. It is essential to estimate mantle temperatures from data independent from gravity, such as seismic tomography. Using these data constrained by mineral physics, we can determine thermal and compositional effects, which control the total density anomaly in the NA continent.

7. Initial Thermal Model

We invert both the regional NA07 and the global SL2013sv tomography model for temperature applying the mineral physics approach of *Stixrude and Lithgow-Bertelloni* [2005], which consists of the evaluation of the physical properties of mantle phases at elevated pressure and temperature using the Eularian finite strain formulation (Appendix A). We used the elastic modulus and the pressure derivative of the mineral phases defined in *Cammarano et al*. [2003], which are estimated taking into account their dependence on the iron content. All the other properties of the mantle, taken from *Stixrude and Lithgow-Bertelloni* [2005], are estimated as a weighted average of the *Mg*, *Fe*, and *Ca* (the latter in case of Gt) species (end-members) composing the olivine (Ol), OPX, CPX, and Gt (Appendix A).

The initial mantle temperature distribution was estimated assuming a uniform composition corresponding to a "fertile" mantle, which experienced a limited amount of melt extraction. This composition is defined as an average of the mineral fractions constituting the "Primitive mantle" rock defined by *McDonough and Sun* [1995] and the "Tecton garnet peridotite" rock of *Griffin et al*. [2003]. Therefore, we used the following mineral modes: Ol: 58.5%, OPX: 15%, CPX: 11.5%, and Gt: 15%. A commonly accepted Mg# for the "Primitive" peridotites (Mg# = 89) is used [e.g., *Lee*, 2003].

The uncertainties affecting the temperatures estimated from the inversion of seismic velocities are difficult to constrain and may largely vary on a regional scale. Apart from the uncertainties related to the compositional choice that might cause an error in temperature by ~200°C [e.g., *Lee*, 2003], in the most depleted part of the craton other uncertainties have to be considered. As pointed out in previous studies [e.g., *Tesauro et al*., 2012a], an uncertainty of the *S* wave velocity of the tomography model used for temperature inversion of 0.05 km/s translates into errors in estimates of temperature up to ~150°C in the cold cratons. However, this uncertainty affects only the areas where data coverage is poor (e.g., the oceans), which are excluded in this study. In other regions, the uncertainty is likely reduced to half of the maximum value, causing errors in estimates of temperature up to ~70°C. The effect is significantly smaller in the hot areas, where velocity variations correspond to smaller temperature changes due to anelasticity. The largest uncertainties of the elastic parameters are those related to their temperature derivatives (with 10% and 20% uncertainties [e.g., *Cammarano et al*., 2003]), leading to uncertainty in the inferred temperatures of about ~70°C above 300 km [*Tesauro et al*., 2010]. The uncertainty of the attenuation model might cause an error in the estimated temperature of ~100°C when the effect of anelasticity becomes pronounced (at temperature >900°C) [e.g., *Jackson et al*., 2002], thus affecting shallow depths only in geothermally warm regions. Its effect increases nonlinearly when the temperature approaches the solidus, such as at the base of the lithosphere or due to the presence of fluids. *Cammarano et al*. [2003] have modeled the anelasticty effect by using simple physical laws that are valid for bulk rock assemblages. We chose the attenuation model Q4 of *Cammarano et al*. [2003] which reproduces this effect more strongly in respect to the other models, and which is more representative for the wet upper mantle. Therefore, both composition and anelasticity models are suitable for a Phanerozoic upper mantle, which is wetter and almost undepleted in *Fe*, Gt, and CPX components with respect to the upper mantle underlying the old cratons. On account of the uncertainties of the attenuation model, the effect of anelasticity might be still underestimated in the areas most strongly affected by partial melt. Another source of uncertainties affecting temperature estimates is seismic anisotropy. Although previous authors have demonstrated that the NA upper mantle is strongly anisotropic [e.g., *Yuan et al*., 2011], this effect is not crucial for this study, since both tomographic models are based on vertically polarized shear waves (see section 4.3).

The thermal models we obtained (Figures 9a and 9b) are based on the two tomography models described above and are identified by the names of these tomographic models, NA07 and SL2013sv, correspondingly. The main difference of the temperatures occurs in the shallow mantle (<100 km) of the cratons. At a depth

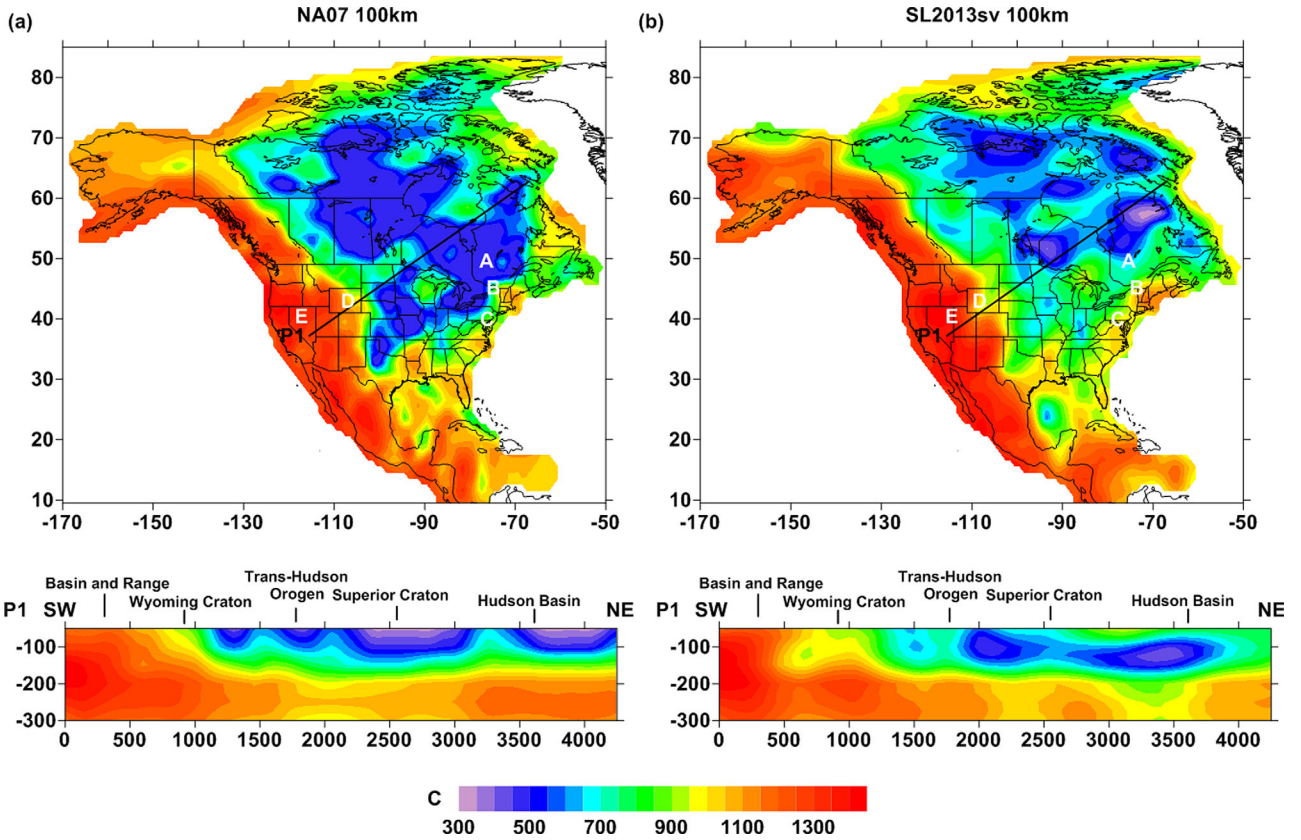

Figure 9. Temperature variations (°C) at a depth of 100 km estimated from the inversion of (a) the regional seismic tomography model NA07 [*Bedle and van der Lee*, 2009] and (b) the global seismic tomography model SL2013sv [*Schaeffer and Lebedev*, 2013], assuming a uniform "Primitive mantle" composition [*Griffin et al.*, 2003; *McDonough and Sun*, 1995] and the anelasticity model Q4 [*Cammarano et al.*, 2003]. The black line shows the cross section location, while the white letters show the locations of the geological provinces whose geotherms are displayed in Figure 10. See text for further explanation.

of 50 km, SL2013sv provides a temperature estimate that is 200°C higher than that estimated using NA07. However, the temperatures according to the former model decrease with increasing depth, causing a negative thermal gradient between 50 and 100 km (see cross sections in Figures 9a and 9b). This effect is due to the relatively low velocities in the shallow upper mantle in model SL2013sv, which might reflect, as before discussed, the effect of the crust not being adequately removed. The temperature differences between the two models tend to be reduced at larger depths and become negligible below 200 km on account of the anelasticity effect. Furthermore, in most of the off-craton areas, the temperatures approach the solidus at a depth shallower than 200 km, while in the coldest parts of the cratons the temperatures reach a maximum of 1100°C in the deep upper mantle. However, we cannot easily estimate the depth of the thermal lithosphere in these regions, since at a depth over 200 km the geotherms are characterized by a constant or negative gradient. These features have been already observed in previous studies [e.g., *Kuskov et al.*, 2014 and references therein] and attributed to an enrichment of the composition in Gt and pyroxenes respect to Ol, starting to occur close to the base of the lithosphere.

Both thermal models show strong temperature differences between the internal part and the western margin of the continent, up to ~700°C at a depth of 100 km. The high temperatures in the NA cordillera (>1200°C at 100 km depth) are in agreement with the high surface heat flow [e.g., *Blackwell and Richards*, 2004] and low resistivity estimated in the same region [e.g., *Rippe et al.*, 2013], suggesting a shallow asthenosphere (<70 km), compared to the adjacent NA craton, the presence of aqueous fluids associated to past subduction [*Hyndman and Currie*, 2011], and a melt fraction of up to 1.5% in the shallow upper mantle [*Rippe et al.*, 2013]. In the southern part, the high temperatures tend to extend to the areas characterized by Proterozoic crust, such as the Colorado Plateau. The high thermal regime in this region possibly originates from thermal warming of the plateau over the last 30–40 Myr, following removal of the Farallon slab

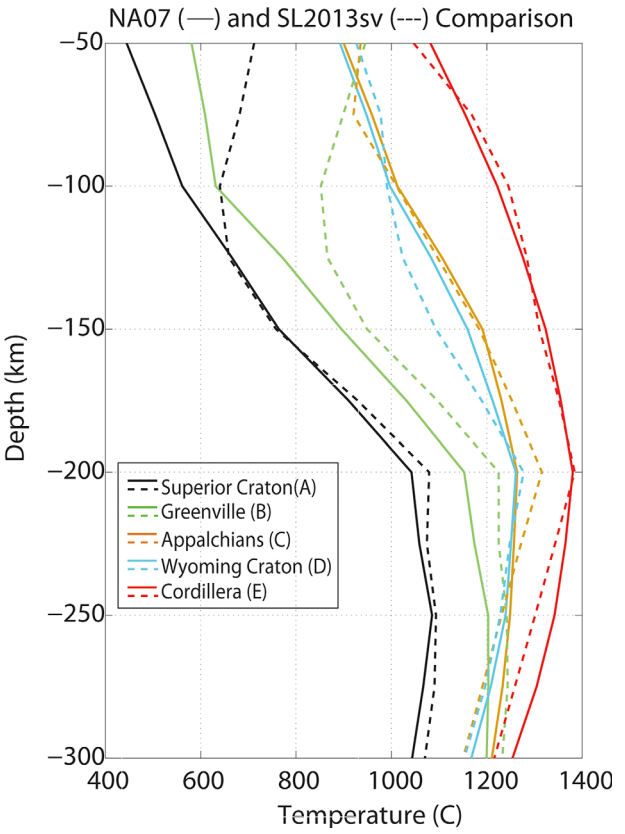

Figure 10. Average mantle temperatures (°C) estimated for selected geological provinces of the NA continent from the inversion of (a) the regional tomography model NA07 [*Bedle and van der Lee*, 2009] and (b) the global tomography model SL2013sv [*Schaeffer and Lebedev*, 2013]. Letters in the legend identify the corresponding geological province and show its location in Figures 9a and 9b.

[*Roy et al*., 2009] or by an upwelling asthenosphere, which progressively infiltrates and replaces the lithosphere, as suggested by previous geophysical studies [e.g., *Schmandt and Humphreys*, 2010; *Crow et al*., 2011].

At the same depth, in the central and eastern parts of the NA continent, the NA07 thermal model shows more homogeneous and on average lower temperatures (∼500°C) compared to SL2013sv (∼600°C). The coldest areas correspond to the Archean Churchill, Slave, and Superior cratons and in part to the Proterozoic terranes. The latter are sometimes characterized by lower temperatures than the Archean regions. For instance, in comparison with the Superior craton, the upper mantle of the Trans-Hudson Orogen, a Paleoproterozoic Orogenic belt, shows temperatures that are either ∼300°C lower (in the NA07 thermal model) or ∼150°C lower (in the SL2013sv thermal model). The temperatures estimated from SL2013sv are more heterogeneously distributed, with the coldest regions (<500°C at a depth of 100 km), as the northwestern part of the Superior craton, of Archean age and most of the Proterozoic areas characterized by temperatures of ∼800°C. Interpretations of the mineralogy of mantle xenoliths [e.g., *Griffin et al*., 2004; *Currie and Hyndman*, 2006; *Hasterok and Chapman*, 2011] predict temperatures between 600°C and 800°C at a depth of 100 km beneath Archean cratons. Thus, the temperatures of both thermal models may be underestimated by ∼100°C or more, likely on account of the uniform, undepleted composition used. In fact, a variation in Mg# by 4–5 units, which corresponds to a typical difference between Archean to Phanerozoic mantle, implies a change of mantle temperature by 200°C [e.g., *Lee*, 2003].

An exception is given by the Wyoming craton, which in both models shows a hot upper mantle (∼1000°C at 100 km), as also observed by *Goes and van der Lee* [2002]. Results from xenoliths interpretations relate such a high thermal regime to Phanerozoic refertilization events, occurring through a prolonged history of both melt removal and melt addition (refertilization) within the shallow part of the lithospheric mantle [e.g., *Carlson et al*., 2004].

A relatively strong temperature difference (∼150°C at 100 km) between the two models is found in the Grenville province (Figure 10) and might be related to the inadequate resolution of the anomalies in a region located at the border of the NA cratons. In the off-cratonic regions, such as the Appalachians, both thermal models show temperatures at 100 km that are ∼350°C higher than older continental interior (Figures 9a, 9b, and 10). The higher mantle temperatures estimated here beneath the Appalachians are in agreement with those estimated by *Goes and van der Lee* [2002] and with a thermal model based on surface heat flow [*Artemieva and Mooney*, 2001]. This region is interpreted as having a hydrated upper mantle associated with the underlying (subducted) Farallon slab [*van der Lee et al*., 2008].

8. Thermal and Compositional Components of the Residual Mantle Gravity Anomalies

To understand the physical origin of the residual mantle gravity and hence the mantle density anomalies, we must first quantify the gravity effect of the temperature variations that have been estimated from the inversion of two seismic tomography models. After subtracting the thermal effect from the residual mantle gravity anomalies, we obtain the temperature-corrected residual field, which corresponds to the compositional component of the density anomaly. This estimated compositional component of the mantle gravity includes uncertainties related to temperature estimations. The latter uncertainties depend on factors that should not exceed $\sim\pm150^{\circ}$C [e.g., *Tesauro et al*., 2012a], which corresponds to a gravity effect of $\sim\pm100$ mGal [*Mooney and Kaban*, 2010].

The effect of both thermal models and the residual "compositional" gravity anomalies are displayed in Figures 11a–11d. The gravity anomalies induced by temperature variations (Figures 11a and 11c) range from about −230 to 370 mGal. The amplitude of these anomalies is at least two times larger than uncertainties of the calculated fields, which combine both the crustal and temperature corrections. Their distributions are relatively uniform and reflect the input thermal models, with large positive anomalies characterizing the upper mantle of the Archean and the Proterozoic cratons and negative values, corresponding to the upper mantle of the central and southern part of the NA Cordillera. Other regions, like the northwestern part of the NA continent show negligible values of thermal gravity anomalies ($<$50 mGal), indicating that the origin of the total mantle anomalies is purely compositional.

The gravity effect of compositional variations spans a range similar to that of the thermal gravity anomalies, from about −370 to 280 mGal, but it is more heterogeneously distributed. Negative anomalies, suggesting a depleted upper mantle, are stronger (locally up to $\sim$100 mGal) in NA07 and extend over the entire cratonic regions, while in SL2013sv they are more localized in the upper mantle of the Canadian Shield. The results obtained from both tomographic models show minima in compositional anomalies (<-250 mGal) in the northwestern part of the Superior craton, in the Slave craton, and the Canadian Proterozoic platform. In the study of *Mooney and Kaban* [2010], the compositional anomalies were estimated only in the central and southern part of the NA continent, according to the geographical limits of the tomography model used (NA00) [*Goes and van der Lee*, 2002]. Therefore, for cratonic regions, we can compare the new results and the previous ones only in the Superior craton. The results are in very good agreement.

Interpretations of the results are somewhat ambiguous in the central part of the U.S., where the compositional anomalies are negative for thermal model NA07 (<-150 mGal), indicative of an upper mantle that is moderately depleted. For thermal model SL2013sv, compositional anomalies are near zero or even positive ($>$150 mGal), in the southern Rocky Mountains, close to the northwestern border of the Colorado plateau. These regions, being mostly of Proterozoic age, might have a more depleted upper mantle, with respect to those of Phanerozoic age, as suggested by NA07. However, the results shown by SL2013sv are similar to those found by *Mooney and Kaban* [2010]. Other maxima, estimated, only in SL2013sv, in the southern part of the U.S., along the border between New Mexico and Texas and in the Grenville province ($>$200 mGal), correspond to those found by these previous authors. Also in this case, we can observe two trends of positive anomalies, the first one, N-S oriented, extends from Texas to the west-central part of Colorado, merging with the second one, NE-SW oriented, and located NW of the Grenville-Appalachian suture. The first anomaly trend, as suggested by *Mooney and Kaban* [2010], might be the effect produced by an upper mantle slab remnant, in accord with the model of *Hildebrand* [2009] that proposes westward-directed subduction ($\sim$150–75 Ma) and slab break off ($\sim$75 Ma) during the evolution of the NA Cordillera. An alternative hypothesis [*Bird*, 1988] explains these anomalies as a result of the advection of the lithospheric mantle originated from the eastward-directed flat slab subduction.

The second broad anomaly (trending NE-SW) might be the effect of slab fragments formed during the closing of the paleo-Atlantic during the early stages of the Appalachian orogeny [e.g., *Thomas*, 1989]. However, we note that in these areas both seismic tomography models provide very weak positive velocity anomalies, indicating that these high-density bodies lack a seismically signature. A similar situation is observed in the Gulf of Mexico and in the southern margin of the NA continent, where the broad positive compositional anomaly ($\sim$150 mGal), estimated from both tomographic models, is not accompanied by high seismic velocities. In fact, as previously discussed, only model SL2013sv gives a small high-velocity anomaly, which

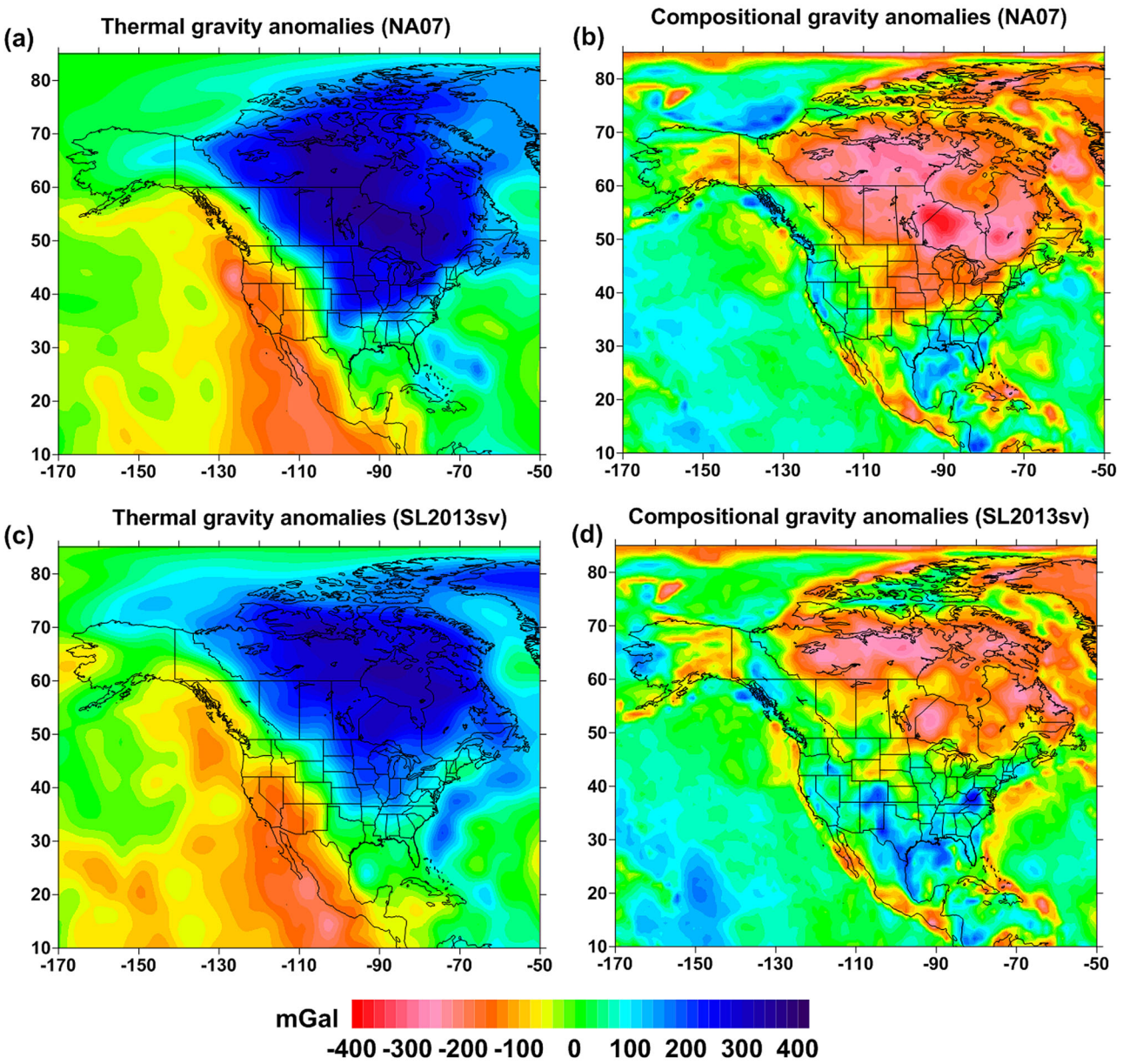

Figure 11. Thermal and compositional component of the mantle gravity anomalies (mGal) estimated using (a and b) the regional tomography model NA07 [*Bedle and van der Lee*, 2009] and (c and d) the global tomography model SL2013sv [*Schaeffer and Lebedev*, 2013]. See text for further explanations.

is located in the west-central part of the Gulf of Mexico, not coinciding with the largest values of the compositional anomalies. It should be noted that it is the compositional anomaly, not the thermal anomaly (Figures 11a and 11c) that accounts for the total gravity anomaly beneath the Gulf of Mexico (Figure 7a). This result suggests that the positive gravity anomaly is caused by a high-density eclogite body, which would explain the subsidence of the Gulf Coast [*Mooney and Kaban*, 2010].

In the NA Cordillera, the compositional anomalies estimated from thermal models NA07 and SL2013sv show a similar trend. They are close to zero in most of this region (Figures 11b and 11d), demonstrating that the mantle gravity anomalies are mainly related to high temperatures, which also supports the high topography. Weak positive anomalies ($<$150 mGal) N-S trending, over Cascade and Sierra Nevada, might reflect the influence of downwelling forces caused by the subducting Juan de Fuca plate that counteracts the upwelling effect of the high temperatures. Relatively large negative values (<-100 mGal) are estimated along the western margin of Mexico, the Gulf of California and Alaska. Since the Phanerozoic upper mantle

of these regions is unlikely to be depleted, it appears likely that the temperature-induced density changes are overestimated, which results in artificial compositional anomalies. Another strong negative compositional anomaly (<-150 mGal) is observed in the southeastern part of Cuba, which might be related to a fragment of depleted African lithosphere [*Mooney and Kaban*, 2010].

9. Conclusions

1. An integrated density model of the upper mantle of North America is constructed based on an improved crustal model and a new gravity inversion technique.
2. The mantle gravity anomalies and residual topography are estimated by removing the crustal effect using an improved density model of sediments [*Mooney and Kaban*, 2010] and NACr14, the most recent crustal model of this region [*Tesauro et al*., 2014a].
3. A new interpretation technique is based on a joint inversion of the gravity anomalies and residual topography. Using these two parameters makes it possible to construct a reliable 3-D density model of the upper mantle.
4. The largest negative mantle anomalies (<-100 mGal) and positive residual topography (up to $\sim$4 km) correspond to the western U.S. (Basin and Range, Mexico, and Gulf of California). These negative gravity anomalies are in agreement with previously reported low P_n velocities and low mantle shear-wave velocities, which indicates their thermal origin. The eastern and central part of the continent is chiefly characterized by positive mantle gravity anomalies and high mantle shear-wave velocities. The largest mantle anomalies ($>$150 mGal) correspond to the Trans-Hudson Orogen and Proterozoic terranes of the U.S. In contrast, the positive mantle anomalies over the younger regions as the Appalachians and the Gulf of Mexico are mostly accompanied by low Pn and shear-wave velocities. These findings support the hypothesis that besides temperature, compositional changes also control the upper mantle density.
5. In western North America, the residual gravity and topography are generally inversely correlated. In contrast, the central and the eastern part of the continent are characterized by negligible ($\pm$0.5) or weakly negative (<-1 km) residual topography, indicating that the crust is almost compensated with respect to the reference model (40 km thick). The Canadian Proterozoic platform and the northwestern part of the Superior Craton are characterized by positive t_{res} (up to 2 km), evidencing that the upper mantle is buoyant in these regions, likely due to depletion.
6. A 3-D density model of the North American mantle is constructed by the inversion of the residual gravity anomalies and residual topography. At a depth of 100 km, the density anomalies are distributed in a similar way to those of the residual gravity anomalies and t_{res} (the last one with the opposite sign). Most of the Western Mesozoic-Cenozoic NA margin is characterized by negative density anomalies (<-0.03 g/cm^3), reflecting the presence of a warm buoyant upper mantle. In contrast, in the inner part of the Colorado Plateau and Cascadia, only weak positive density anomalies are observed, indicating that the possible effect of high temperatures is largely compensated by that of composition, which might be related to a cold subducting slab. Large positive density anomalies estimated for the Proterozoic upper mantle might be interpreted as the effect of relatively low temperatures and weak depletion of the upper mantle material. On the other hand, the Archean Superior craton and the Proterozoic Canadian platform are characterized by negligible density anomalies, suggesting that the effect of composition and temperature in this case counteract each other. The positive density variations tend to fade with depth, becoming negligible below 250 km ($<$0.005 g/cm^3), while the negative ones extend in the deeper layers of the upper mantle.
7. In order to separate (to first order) the thermal and compositional components of the residual mantle gravity anomalies and residual topography, we estimate temperatures (T) by inverting two recent seismic tomography models, NA07 [*Bedle and van der Lee*, 2009] and SL2013sv [*Schaeffer and Lebedev*, 2013]. By considering two tomography models, we can estimate ambiguities that arise due to uncertainties of seismic tomography. When converting V_s to T, a uniform composition is used ("fertile" composition and the anelasticity model Q3) [*Cammarano et al*., 2003], which is representative of the Phanerozoic mantle. The thermal obtained models show large differences between the internal part and the western margin of the continent (up to 700°C at a depth of 100 km). The high temperatures in NA Cordillera tend to extend to the east in the Proterozoic Colorado Plateau and in the Archean Wyoming craton. The high thermal regime possibly corresponds to a slabless window appeared after removal

of the Farallon slab [*Roy et al*., 2009] or from an upwelling asthenosphere, progressively replacing the lithosphere [e.g., *Schmandt and Humphreys*, 2010; *Crow et al*., 2011]. In contrast, the high temperatures in the Wyoming craton are likely related to Phanerozoic refertilization events [e.g., *Carlson et al*., 2004]. The coldest areas (∼500°C at a depth of 100 km) correspond in both models to the Archean cratons (Churchill, Slave, and Superior). The Proterozoic upper mantle is also characterized by low temperatures according to the NA07 model, while has relatively high temperatures (800°C) according to SL2013sv (e.g., in the Grenville province). Such differences might be due to the different resolution of the models at the border of the NA cratons.

8. Using the initial thermal models, we estimate the thermal component of the residual mantle gravity anomalies and we subtract them from the total anomalies in order to get residuals, which likely correspond to compositional anomalies and to the uncertainties of the estimated temperatures. After removing of the effect of temperature variations, the compositional residual gravity anomalies and residual topography are estimated. The compositional residual anomalies are more heterogeneously distributed than the total mantle fields. Negative anomalies, indicating a depleted upper mantle are extended over the entire cratonic region in NA07, while in SL2013sv they are localized in the Canadian Shield, northwestern part of the Superior Craton, Slave craton, and the Canadian Proterozoic Platform. In SL2013sv are observed two trends of positive anomalies (>200 mGal); the first one, N-S oriented, is extended from Texas to the central-western part of Colorado, merging the second one, which is NE-SW oriented northwest of the Grenville-Appalachian suture. These anomalies might reflect the effect of fragments of the slabs formed during the evolution of the NA Cordilera and of the Appalachians [e.g., *Hildebrand*, 2009; *Thomas*, 1989]. Alternatively, they might be interpreted as a result of the advection of the lithospheric mantle [e.g., *Bird*, 1988]. A broad positive anomaly (∼150 mGal) is observed in both models in the Gulf of Mexico and, as was suggested by *Mooney and Kaban* [2010], it might be related to an eclogite body, which is often seismically indistinguishable in the upper mantle. In NA Cordillera the compositional anomalies are mostly negligible, showing that the total mantle gravity is chiefly due to the high temperatures. The weak positive anomalies observed in Cascadia and Sierra Nevada (<150 mGal) are possibly associated with the subducting Juan de Fuca plate.
9. The results obtained in this study help to identify the origin of the upper mantle heterogeneity. However, evaluating temperatures with the uniform "fertile" composition, as is done here, might bias the estimates especially in the cratonic regions. In Part 2 [*Tesauro et al*., 2014b], we evaluate the effect of mantle depletion beneath cratons by applying an iterative technique.

Appendix A

Mineral Physics Approach

To invert the seismic velocity in temperature, we estimate the anharmonic velocity of a peridotite containing four main mineral phases (Ol, OPX, CPX, and Gt). Each one is treated as an ideal solid solution of *Mg* and *Fe* species (end-members) and in case of Gt also of *Ca* species (end-member): Ol (forsterite + fayalite), OPX (enstatite), CPX (diopside + hedenbergite), Gt (pyrope + almandine + glossular). The percentage of the main mineral phases varies, as well as the percentage of *Fe* and *Mg* species, by varying the Mg # (section 7). The amount of *Ca* end-member of the Gt (glossular) is taken constant (20%). The bulk and the shear modulus (K_0 and G_0) and the pressure derivative of each mineral phase at zero pressure (P_0) and room temperature ($T_0 = 300$ K) (STP conditions) are taken from *Cammarano et al*. [2003] (In the equations. displayed subscript "0" refers to STP conditions). All the other parameters displayed in the equations below of each end-member at the same STP conditions are taken from *Stixrude and Lithgow-Bertelloni* [2005] (Table A1).

To estimate the bulk and shear modulus of each mineral phase as a function of temperature and pressure, we express the total pressure, $P_{TOT}(V,T)$, as a sum of the pressure at reference temperature, P_{ref} (e.g., isothermal compression at 300 K), and the thermal pressure, which increases along an isochore, ΔP_{th}:

$$P_{TOT}(V,T) = P_{ref}(V) + \Delta P_{th}(V,T). \quad \text{(A1)}$$

Isothermal compression is estimated through the third-order Birch-Murnaghan equation (For the explicit form of the equation see *Stixrude and Lithgow-Bertelloni* [2005].)

Table A1. Properties of Mantle Species Used in This Study

Mineral Phases	Species	Formula	V_o cm^3/mol	K_o GPa	K_0'	θ_0 K$_0$	$\gamma 0$	q	G_o GPa	G_0'	$\eta_s 0$
Olivine	Forsterite	Mg_2SiO_4	43.60	129	4.2	809	0.99	2.1	81-31X_{Fe}	1.4	2.4
	Fayalite	Fe_2SiO_4	46.29			619	1.06	3.6			1.1
OPX	Enstatite	$Mg_4Si_4O_{12}$	125.35	109+20X_{Fe}	7.0	810	0.67	7.8	75+10X_{Fe}	1.6	2.4
	Ferrosilite	$Fe_4Si_4O_{12}$	131.88			680	0.67	7.8			1.1
CPX	Diopside	$Ca_2Mg_2Si_4O_{12}$	132.08	105+12X_{Fe}	6.2-1.9X_{Fe}	782	0.96	1.5	67-6X_{Fe}	1.7	1.6
	Hedenbergite	$Ca_2Fe_2Si_4O_{12}$	135.73			702	0.93	1.5			1.6
Garnet	Pyrope	$Mg_3Al_2Si_3O_{12}$	113.08	171+15X_{Fe}	4.4	823	1.01	1.4	92+7X_{Fe}	1.4	1.0
	Almandine	$Fe_3Al_2Si_3O_{12}$	115.43			742	1.10	1.4			2.2
	Grossular	$Ca_3Al_2Si_3O_{12}$	125.12			823	1.08	0.4			2.4

$$P_{st}=\frac{3}{2}K_{T_0}\left[\left(\frac{V_0}{V}\right)^{\frac{7}{3}}-\left(\frac{V_0}{V}\right)^{\frac{5}{3}}\right]\left\{1-\frac{3}{4}\left(4-K_{T_0}'\right)\left[\left(\frac{V_0}{V}\right)^{\frac{2}{3}}-1\right]\right\}, \tag{A2}$$

where V is the molar volume at the temperature considered (T). The thermal pressure can be described using the Debye model [*Jackson and Rigden*, 1996]:

$$\Delta P_{th}=\frac{\gamma(V)}{V}\left[E_{th}(V,T)-E_{th}(V,T_0)\right], \tag{A3}$$

where γ is the Grüneisen parameter, which describes the effect that changing the volume of a crystal lattice has on its vibrational properties, and, as a consequence, the effect that changing temperature has on the size or dynamics of the lattice. It is assumed to have the form:

$$\gamma=\gamma_0\left(\frac{V}{V_0}\right)^q, \tag{A4}$$

where q is the volume dependence of the Grüneisen parameter ($q=dln\gamma/dlnV$), which is assumed to be constant for each end-member [*Stixrude and Lithgow-Bertelloni*, 2005].

E_{th} is the vibrational energy for a given volume and temperature, which can be calculated from the Debye model:

$$E_{th}=\frac{9nRT}{(\theta/T)^3}\int_0^{\theta/T}\frac{x^3dx}{e^x-1}, \tag{A5}$$

where $\frac{3}{(\theta/T)^3}\int_0^{\theta/T}\frac{x^3dx}{e^x-1}$ is the Debye function (with θ the Debye temperature (A10)), R the gas constant, n the number of atoms per formula unit.

The isentropic bulk modulus as function of temperature and pressure, corrected for the difference between isothermal and isentropic values is given by:

$$K=K_T(1+\alpha\gamma T), \tag{A6}$$

where α the thermal expansion coefficient is:

$$\alpha=\gamma C_v/K_T V, \tag{A7}$$

and K_T is

$$K_T(V,T)=K_0(1+2f)^{5/2}[1+(3K_0'-5)f+27/2(K_0'-4)f^2]+(\gamma/V)(\gamma+1-q)E_{th}(V,T)-E_{th}(V,T_0)-(\gamma^2/V),\left(TC_{v(V,T)}-300C_{v(V,300k)}\right) \tag{A8}$$

which agrees with the expression to third order derived from a purely isotropic thermodynamic analysis [*Stixrude and Lithgow-Bertelloni*, 2005].

In (A7) and (A8), Cv is the heat capacity at constant volume:

$$C_v=(dE_{th}/dT)_v=4E_{th}/T-9nR(\theta/T)/[\exp(\theta/T)-1], \tag{A9}$$

where θ, the Debye temperature, is estimated as:

$$\theta=\theta_0 Exp\left(\frac{\gamma_0-\gamma(V)}{q}\right). \tag{A10}$$

In (A8), $K_0^{'}$is the pressure derivative of the bulk modulus K_0 and f is:

$$f=\frac{1}{2}\left[\left(\frac{V_0}{V}\right)^{2/3}-1\right]. \tag{A11}$$

The shear modulus as a function of temperature and pressure is given by:

$$G(V,T)=(1+2f)^{5/2}\left[G_0+\left(3K_0G_0^{'}-5G_0\right)f+\left(6K_0G_0^{'}-24K_0-14G_0+\frac{9}{2}K_0K_0^{'}\right)f^2\right]-\eta_s\frac{E_{th}(V,T)-E_{th}(V,T_0)}{V}, \tag{A12}$$

where $G_0^{'}$ is the pressure derivative of the shear modulus G_0 and η is the shear strain derivative of γ *[Stixrude and Lithgow-Bertelloni*, 2005].

$$\eta_s=\eta_{s0}\left(\frac{V}{V_0}\right). \tag{A13}$$

The density as a function of temperature and pressure is estimated dividing the molar mass (m) by the molar volume (V)

$$\rho=\left(\frac{m}{V}\right). \tag{A14}$$

Once we estimated the anharmonic velocities of the peridotite, we applied the anelastic correction using an attenuation model (in this study Q4 from *Cammarano et al*. [2003]).

Acknowledgments
The data presented in the paper are available upon request. We thank two anonymous reviewers and the Editor Cin-Ty A. Lee for their extensive reviews that have greatly improved the manuscript. The paper also benefited from the discussion with Sergio Speziale regarding mineral physics. This study was funded by the Alexander von Humboldt Foundation postdoctoral grant (M.T.) and Award (S.C.), GeoForschungsZentrum, Potsdam, Utrecht University, the Netherlands Research Centre for Integrated Solid Earth (ISES), and the USGS National Earthquake Hazards Reduction Program.

References

Afonso, J. C., G. Ranalli, M. Fernàndez, W. L. Griffin, S. Y. O'Reilly, and U. Faul (2010), On the Vp/Vs - Mg# correlation in mantle peridotites: Implications for the identification of thermal and compositional anomalies in the upper mantle, *Earth Planet. Sci. Lett.*, *289*, 606–610.

Artemieva, I. M., and W. D. Mooney (2001), Thermal thickness and evolution of Precambrian lithosphere: A global study, *J. Geophys. Res.*, *106*(B8), 16,387–16,414.

Artemjev, M. E., and M. K. Kaban (1994), Density inhomogeneities, isostasy and flexural rigidity of the lithosphere in the Transcaspian region, *Tectonophysics*, *240*, 281–297.

Bassin, C., G. Laske, and G. Masters (2000), The current limits of resolution for surface wave tomography in North America, *Eos Trans. AGU*, *81*(48), Fall Meet. Suppl., Abstract S12A-03.

Becker, T. W. (2012), On recent seismic tomography for the western United States, *Geochem. Geophys. Geosyst.*, *13*, Q01W10, doi:10.1029/2011GC003977.

Becker, T. W., C. Faccenna, E. D. Humphreys, A. R. Lowry and M. S. Miller (2014), Static and dynamic support of western United States topography, *Earth Planet. Sci. Lett.*, *402*, 234–246.

Bedle, H., and S. van der Lee (2006), Fossil flat-slab subduction beneath the Illinois basin, USA, *Tectonophysics*, *424*(1–2), 53–68.

Bedle, H., and S. van der Lee (2009), *S* velocity variations beneath North America, *J. Geophys. Res.*, *114*, B07308, doi:10.1029/2008JB005949.

Bird, P. (1988), Formation of the Rocky Mountains, western United States: A continuum computer model, *Science*, *239*, 1501–1507, doi:10.1126/science.239.4847.1501.

Blackwell, D. D., and M. Richards (2004), *Geothermal map of North America, sheet 1, scale 1:6,500,000*, Am. Assoc. of Pet. Geol., Tulsa, Okla.

Bleeker, W. (2003), The late Archean record: A puzzle in ca. 35 pieces, *Lithos*, *71*, 99–134.

Boschi, L., C. Faccenna, and T. W. Becker (2010), Mantle structure and dynamic topography in the Mediterranean Basin, *Geophys. Res. Lett.*, *37*, L20303, doi:10.1029/2010GL045001.

Cammarano, F., S. Goes, P. Vacher, and D. Giardini (2003), Inferring upper-mantle temperatures from seismic velocities, *Phys. Earth Planet. Inter.*, *138*, 197–222, doi:10.1016/S00319201(03)00156-0.

Cammarano, F., F. Tackley, and L. Boschi (2011), Seismic, petrological and geodynamical constraints on thermal and compositional structure of the upper mantle: Global thermo-chemical models, *Geophys. J. Int.*, *187*, 1301–1318.

Carlson, R. W., I. J. Irving, D. J. Schulze, and B. C. Hearn (2004), Timing of Precambrian melt depletion and Phanerozoic refertilization events in the lithospheric mantle of the Wyoming Craton and adjacent Central Plains Orogen, *Lithos*, *77*, 453–472.

Christensen, N. I., and W. D. Mooney (1995), Seismic velocity structure and composition of the continental crust: A global review, *J. Geophys. Res.*, *100*(B6), 9761–9788.

Collins, C. D. N., B. J. Drummond, and M. G. Nicoll (2003), Crustal thickness patterns in the Australian continent, *Spec. Pap. Geol. Soc. Am.*, *372*, 121–128.

Crow, R., K. Karlstrom, Y. Asmerom, B. Schmandt, V. Polyaka, and S. A. DuFrane (2011), Shrinking of the Colorado Plateau via lithospheric mantle erosion: Evidence from Nd and Sr isotopes and geochronology of Neogene basalts, *Geology*, *39*, 27–30, doi:10.1130/G31611.1.

Currie, C. A., and R. D. Hyndman (2006), The thermal structure of subduction zone back arcs, *J. Geophys. Res.*, *111*, B08404–30, doi:10.1029/7492005JB004024.
Deschamps, F., J. Trampert, and R. Snieder (2002), Anomalies of temperature and iron in the uppermost mantle inferred from gravity data and tomographic models, *Phys. Earth Planet. Inter.*, *129*, 245–264.
Deuss, A. (2009), Global observations of mantle discontinuities using SS and PP precursors, *Surv. Geophys.*, *30*, 301–326.
Dickinson, W. R. (2004), Evolution of the North American Cordillera, *Annu. Rev. Earth Planet. Sci.*, *32*, 13–45, doi:10.1146/annurev.earth.32.101802.120257.
Dziewonski, A., and D. Anderson (1981), Preliminary reference earth model, *Phys. Earth Planet. Inter.*, *25*, 297–356.
Dziewonski, A., A. Hales, and E. Lapwood (1975), Parametrically simple Earth models consistent with geophysical data, *Phys. Earth Planet. Inter.*, *10*(1), 12–48.
Faccenna, C., and T. W. Becker (2010), Shaping mobile belts by small-scale convection, *Nature*, *465*, 602–605, doi:10.1038/nature09064.
Förste, C., et al. (2011), EIGEN-6—A new combined global gravity field model including GOCE data from the collaboration of GFZ-Potsdam and GRGS-Toulouse, *Geophys. Res. Abstr.*, *13*, EGU Gen. Assem., Abstract EGU2011–3242-2.
Forte, A. M., and W. R. Peltier (1991), Viscous flow models of global geophysical observables: 1. Forward problems, *J. Geophys. Res.*, *96*(B12), 20,131–20,159.
Ghosh, A., T. W. Becker and E. D. Humphreys (2013), Dynamics of the North American continent, *Geophys. J. Int.*, *194*, 651–669.
Godey, S., R. Sneider, A. Villasenor, and H. Benz (2003), Surface wave tomography of North America and the Caribbean using global and regional broadband networks: Phase velocity maps and limitations of ray theory, *Geophys. J. Int.*, *152*(3), 629–623.
Godey, S., F. Deschamps, J. Trampert, and R. Sneider (2004), Thermal and compositional anomalies beneath the North American continent, *J. Geophys. Res.*, *109*, B01308, doi:10.1029/2002JB002263.
Goes, S., and S. van der Lee (2002), Thermal structure of the North American uppermost mantle inferred from seismic tomography, *J. Geophys. Res.*, *107*(B3), doi:10.1029/2000JB000049.
Goes, S., R. Govers, and P. Vacher (2000), Shallow upper mantle temperatures under Europe from P and S wave tomography, *J. Geophys. Res.*, *105*(11), 11,153–11,169.
Grand, S. (1994), Mantle shear structure beneath the Americas and surrounding oceans, *J. Geophys. Res.*, *99*(B6), 11,591–11,621, doi:10.1029/94JB00042.
Griffin, W. L., S. Y. O'Reilly, N. Abe, S. Aulback, R. M. Davies, N. J. Pearson, B. J. Doyle, and K. Kivi (2003), The origin and evolution of Archean lithospheric mantle, *Precambrian Res.*, *127*, 19–41.
Griffin, W. L., S. Y. O'Reilly, B. J. Doyle, N. J. Pearson, H. Coopersmith, K. Kivi, V. Malkovets, and N. Pokhilenk (2004), Lithosphere mapping beneath the North American plate, *Lithos*, *77*, 873–922.
Hasterok, D., and D. S. Chapman (2011), Heat production and geotherms for the continental lithosphere, *Earth Planet. Sci. Lett.*, *307*, 59–70.
Hieronymous, C. F., and S. Goes (2010), Complex cratonic seismic structure from thermal models of the lithosphere: Effects of variations in deep radiogenic heating, *Geophys. J. Int.*, *180*, 999–1012, doi:10.1111/j.1365-246X.2009.04478.x.
Hildebrand, R. S. (2009), Did westward subduction cause Cretaceous-Tertiary orogeny in the North American cordillera?, *Spec. Pap. Geol. Soc. Am.*, *457*, 1–71.
Hoffman, P. F. (1997), *Tectonic genealogy of North America, in* Earth Structure: An Introduction to Structural Geology and Tectonics, edited by B. A. van der Pluijm and S. Marshak, pp. 459–464, McGraw-Hill, N. Y.
Hyndman, R. D., and C. A. Currie (2011), Why is the North America Cordillera high? Hot backarcs, thermal isostasy, and mountain belts, *Geology*, *39*, 783–786.
Jackson, I., and S. M. Rigden (1996), Analysis of P-V-T data; constraints on the thermoelastic properties of high-pressure minerals, *Phys. Earth Planet. Inter.*, *96*, 85–112.
Jackson, I., J. D. F. Gerald, U. H. Faul, and B. H. Tan (2002), Grain-size-sensitive seismic wave attenuation in polycrystalline olivine, *J. Geophys. Res.*, *107*(B12), 2360, doi:10.1029/2001JB001225.
Jordan, T. H. (1979), Mineralogies, densities and seismic velocities of garnet lherzolites and their geophysical implications, in *The Mantle Sample: Inclusions in Kimberlites and Other Volcanics*, edited by F. R. Boyd and H. O. A. Meyer, pp. 1–14, AGU, Washington, D. C.
Kaban, M. K. (2011), Gravity anomalies, interpretation, in *Encyclopedia of Solid Earth Geophysics*, 2nd ed., edited by H. K. Gupta, pp. 456–461, Springer, Berlin.
Kaban, M. K., P. Schwintzer, and P. S. A. Tikhotsky (1999), Global isostatic gravity model of the Earth, *Geophys. J. Int.*, *136*, 519–536.
Kaban, M. K., P. Schwintzer, I. M. Artemieva, and W. D. Mooney (2003), Density of the continental roots: Compositional and thermal contributions, *Earth Planet. Sci. Lett.*, *209*, 53–69.
Kaban, M. K., P. Schwintzer, and Ch. Reigber (2004), A new isostatic model of the lithosphere and gravity field, *J. Geod.*, *78*, 368–385.
Kaban, M. K., M. Tesauro, and S. Cloetingh (2010), An integrated gravity model for Europe's crust and upper mantle, *Earth Planet. Sci. Lett.*, *296*, 195–209.
Kaban, M. K., A. Petrunin, and W. Mooney (2013), *Cratonic roots under North America are shifted by basal drag: New evidence from gravity and geodynamic modeling*, Abstract T21C-05 presented at 2013 Fall Meeting, AGU, San Francisco, Calif., 9–13 Dec.
Karlstrom, K., and E. Humphreys (1998), Persistent influence of Proterozoic accretionary boundaries in the tectonic evolution of southwestern North America: Interaction of cratonic grain and mantle modification events, *Rocky Mt. Geol.*, *33*(2), 161–179.
Kennett, B. L. N., E. R. Engdahl, and R. Buland (1995), Constraints on seismic velocities in the Earth from travel times, *Geophys. J. Int.*, *122*(1), 108–124.
Khan, A., A. Zunino, and F. Deschamps (2011), The thermo-chemical and physical structure beneath the North American continent from Bayesian inversion of surface-wave phase velocities, *J. Geophys. Res.*, *116*, B09304, doi:10.1029/2011JB008380.
Kuskov, O. L., V. A. Kronrod, A. A. Prokofyev, and N. I. Pavlenkova (2014), Thermo-chemical structure of the lithospheric mantle underneath the Siberian craton inferred from long-range seismic profiles, *Tectonophysics*, *615–616*, 154–166.
Laske, G., G. Masters, Z. Ma, and M. Pasyanos (2013), Update on CRUST1.0—A 1-degree global model of Earth's crust, *Geophys. Res. Abstr.*, *15*, EGU Gen. Assemb., Abstract EGU2013–2658.
Lee, C.-T. (2003), Compositional variation of density and seismic velocities in natural peridotites at STP conditions: Implications for seismic imaging of compositional heterogeneities in the upper mantle, *J. Geophys. Res.*, *108*(B9), 2441, doi:10.1029/2003JB002413.
Levander, A., B. Schmandt, M. S. Miller, K. Liu, K. E. Karlstrom, R. S. Crow, C.-T. Lee, and E. D. Humphreys (2011), Regional Colorado Plateau uplift by delamination and thermo-chemical downwelling of North American lithosphere, *Nature*, *472*, 461–465.
Liu, L., and M. Gurnis (2010), Dynamic subsidence and uplift of the Colorado Plateau, *Geology*, *38*, 663–666.
Marone, F., Y. Gung, and B. Romanowicz (2007), Three-dimensional radial anisotropic structure of the North American upper mantle from inversion of surface waveform data, *Geophys. J. Int.*, *171*, 206–222, doi:10.111/j.1365-246X.2007.03465.x.

McDonough, W. F., and S.-S. Sun (1995), The composition of the Earth, *Chem. Geol.*, *120*, 223–253.
McQuarrie, N., and M. Oskin (2010), Palinspastic restoration of NAVDat and implications for the origin of magmatism in southwestern North America, *J. Geophys. Res.*, *115*, B10401, doi:10.1029/2009JB006435.
Mooney, W. D. (2014), Global crustal structure, in *The Treatise of Geophysics*, vol. 1, 2nd ed., *Crust and Mantle*, edited by B. Romanowicz, A. Dziewonski, and G. Schubert, pp. 361–417, Elsevier, Amsterdam.
Mooney, W. D., and M. K. Kaban (2010), The North American upper mantle: Density, composition, and evolution, *J. Geophys. Res.*, *115*, B12424, doi:10.1029/2010JB000866.
Moucha, R., A. M. Forte, D. B. Rowley, J. X. Mitrovica, N. A. Simmons, and S. P. Grand (2009), Deep mantle forces and the uplift of the Colorado Plateau, *Geophys. Res. Lett.*, *36*, L19310, doi:10.1029/2009GL039778.
Nettles, M., and A. Dziewonski (2008), Radially anisotropic shear velocity structure of the upper mantle globally and beneath North America, *J. Geophys. Res.*, *113*, B02303, doi:10.1029/2006JB004819.NOAA (2010), [Aailable at http://www.ngdc.noaa.gov/mgg/sedthick/sedthick.html.]
Nolet, G. (1990), Partitioned waveform inversion and two-dimensional structure under the network of autonomously recording seismographs, *J. Geophys. Res.*, *95*(B6), 8499–8512.
Nolet, G., C. Coutlee, and B. Clouser (1998), Sn velocities in western and eastern North America, *Geophys. Res. Lett.*, *25*(10), 1557–1561.
Parsons, T., G. A. Thompson, and N. H. Sleep (1994), Mantle plume influence on the Neo gene uplift and extension of the U.S. western Cordillera, *Geology*, *22*, 83–86.
Petrunin, A. G., M. K. Kaban, I. Rogozhina, and V. Trubitsyn (2013), Revising the spectral method as applied to modeling mantle dynamics, *Geochem. Geophys. Geosyst.*, *14*, 3691–3702, doi:10.1002/ggge.20226.
Rippe, D., M. J. Unsworth, and C. A. Currie (2013), Magnetotelluric constraints on the fluid content in the upper mantle beneath the southern Canadian Cordillera: Implications for rheology, *J. Geophys. Res. Solid Earth*, *118*, 1–24, doi:10.1002/jgrb.50255.
Ritsema, J., A. Deuss, H. J. van Heijst, and J. H. Woodhouse (2011), S40RTS: A degree-40 shear-velocity model for the mantle from new Rayleigh wave dispersion, teleseismic traveltime and normal-mode splitting function measurements, *Geophys. J. Int.*, *184*(3), 1223–1236.
Roy, M., T. H. Jordan, and J. Pederson (2009), Colorado Plateau magmatism and uplift by warming of heterogeneous lithosphere, *Nature*, *459*, 978–982, doi:10.1038/nature08052.
Schaeffer, A. J., and S. Lebedev (2013), Global shear-speed structure of the upper mantle and transition zone, *Geophys. J. Int.*, *194*(1), 417–449.
Schmandt, B., and E. Humphreys (2010), Complex subduction and small-scale convection revealed by body wave tomography of the western United States, *Earth Planet. Sci. Lett.*, *297*, 435–445, doi:10.1016/j.epsl.2010.06.047.
Shen, W., M. H. Ritzwoller, and V. Schulte-Pelkum(2013), A 3-D model of the crust and uppermost mantle beneath the Central and Western US by joint inversion of receiver functions and surface wave dispersion, *J. Geophys. Res. Solid Earth*, *118*, 1–15, doi:10.1029/2012JB009602.
Steinberger, B., and A. R. Calderwood (2006), Models of large-scale viscous flow in the Earth's mantle with constraints from mineral physics and surface observations, *Geophys. J. Int.*, *167*, 1461–1481.
Stixrude, L., and C. Lithgow-Bertelloni (2005), Thermodynamics of mantle minerals—I. Physical properties, *Geophys. J. Int.*, *162*, 610–632.
Stolk, W., M. Kaban, F. Beekman, M. Tesauro, W. D. Mooney, and S. Cloetingh (2013), High resolution regional crustal models from irregularly distributed data: Application to Asia and adjacent areas, *Tectonophysics*, *602*, 55–68.
Strakhov, V. N., T. V. Romaniuka, and N. K. Frolova (1989), Method of direct gravity problem solution for modeling of global and regional gravity anomalies [in Russian], in *New Methods of the Gravity and Magnetic Anomaly Interpretation*, edited by V. Strakhov, pp. 118–235, Inst. Phys. of the Earth, Moscow.
Tesauro, M., M. K. Kaban, and S. A. P. L. Cloetingh (2008), EuCRUST-07: A new reference model for the European crust, *Geophys. Res. Lett.*, *35*, L05313, doi:10.1029/2007GL032244.
Tesauro, M., M. K. Kaban, and S. A. P. L. Cloetingh (2010), Thermal and rheological model of the European lithosphere, in New Frontiers in Integrated Solid Earth Sciences, edited by S. A. P. L. Cloetingh and J. F. W. Negendank, pp. 71–101, Springer, Berlin.
Tesauro, M., P. Audet, M. K. Kaban, R. Bürgmann, and S. A. P. L. Cloetingh (2012a), The effective elastic thickness of the continental lithosphere: Comparison between rheological and inverse approaches, *Geochem. Geophys. Geosyst.*, *13*, Q09001, doi:10.1029/2012GC004162.
Tesauro, M., M. K. Kaban, and S. A. P. L. Cloetingh (2012b), Global strength and elastic thickness of the lithosphere, *Global Planet. Change*, *90–91*, 51–57.
Tesauro, M., M. K. Kaban, W. D. Mooney, and S. A. P. L. Cloetingh (2014a), A 3D model for the crustal structure of the North American Continent, *Tectonophysics*, *631*, 65–86.
Tesauro, M., M. K. Kaban, W. D. Mooney, and S. A. P. L. Cloetingh (2014b), Density, temperature, and composition of the North American lithosphere—New insights from a joint analysis of seismic, gravity, and mineral physics data: 2. Thermal and compositional model of the upper mantle, *Geochem. Geophys. Geosyst.*, *15*, 4808–4830, doi:10.1002/2014GC005484.
Thomas, W. A. (1989), The Appalachian-Ouachita Orogen beneath the Gulf Coastal Plain between the outcrops in the Appalachian and Ouachita Mountains, in *The Appalachian-Ouachita Orogen in the United States, Geology of North America*, vol. F-2, edited by R. D. Hatcher Jr., W. A. Thomas and G. W. Viele, pp. 537–553, Geol. Soc. of Am., Boulder, Colo.
Tikhonov, A. N., and V. Y. Arsenin (1977), *Solutions of Ill-Posed Problems*, edited by V. H. Winston, 258 p., John Wiley, N. Y.
van der Lee, S., and A. Frederiksen (2005), Surface wave tomography applied to the North American upper mantle, in *Seismic Earth: Array Analysis of Broadband Seismograms, Geophys. Monogr. Ser.*, vol. 157, edited by A. Levander and G. Nolet, pp. 67–80, AGU, Washington, D. C.
van der Lee, S., and G. Nolet (1997), Upper mantle S velocity structure of North America, *J. Geophys. Res.*, *102*(10), 22,815–22,838.
van der Lee, S., K. Regenauer-Lieb, and D. A. Yuen (2008), The role of water in connecting past and future episodes of subduction, *Earth Planet. Sci. Lett.*, *273*, 15–27.
van Wijk, J., W. S. Baldridge, J. van Hunen, S. Goes, R. Aster, D. D. Coblentz, S. P. Grand, and J. Ni (2010), Small-scale convection at the edge of the Colorado Plateau: Implications for topography, magmatism, and evolution of Proterozoic lithosphere, *Geology*, *38*(7), 611–614, doi:10.1130/G31031.1.
Visser, K., J. Trampert, and B. L. N. Kennett (2008), Global anisotropic phase-velocity maps for higher mode Love and Rayleigh waves, *Geophys. J. Int.*, *172*, 1016–1032.
Yuan, H., B. Romanowicz, K. M. Fischer, and D. Abt (2011), 3-D shear wave radially and azimuthally anisotropic velocity model of the North American upper mantle, *Geophys. J. Int.*, *184*, 1237–1260.